

The Environments of Ultra-strong Mg II Absorbers¹

Daniel B. Nestor²

Department of Astronomy, University of Florida, Gainesville, FL, 32611

Institute of Astronomy, Madingley Road, Cambridge CB3 0HA, UK

and

David A. Turnshek², Sandhya M. Rao², and Anna M. Quider

Department of Physics & Astronomy, University of Pittsburgh, Pittsburgh, PA 15260

ABSTRACT

We present r' - or i' -band WIYN images of the fields of 15 Sloan Digital Sky Survey quasars that have spectra exhibiting intervening Mg II absorption-line systems with rest equivalent widths $2.7 \text{ \AA} \leq W_0^{\lambda 2796} \leq 6.0 \text{ \AA}$ and redshifts $0.42 < z_{\text{abs}} < 0.84$. Such systems are rare and exhibit projected absorption velocity spreads in excess of $\approx 300\text{--}650 \text{ km s}^{-1}$. Approximately 60% are expected to be damped Ly α systems. In each of our fields we detect at least one galaxy that, if at the absorption redshift, would have impact parameter $b \lesssim 40 \text{ kpc}$ and luminosity $L \gtrsim 0.3L^*$. We measure a significant excess of galaxies at low- b to the sightlines over a large range of luminosity. Many of the sightlines are found to pass either through or close to the optically-luminous extent of a galaxy. Considering the very large velocity spreads seen in absorption, this suggests that these absorbing regions are more kinematically complex than local spirals such as the Milky Way. Our data indicate that interactions and galaxy pairs may be a contributing factor to the production of such large velocity spreads. Finally, we also find evidence that a population of galaxies with luminosities in the range $4L^* \lesssim L \lesssim 13L^*$ may contribute to the presence of ultra-strong Mg II absorption. Thus, some of the absorbing galaxies may represent a population intermediate to the very luminous high-redshift Lyman break galaxies and the fainter local starburst population.

¹Based on data obtained from the Sloan Digital Sky Survey (SDSS) and the WIYN³ telescope.

²Visiting Astronomer, Kitt Peak National Observatory, National Optical Astronomy Observatory, which is operated by the Association of Universities for Research in Astronomy, Inc. (AURA) under cooperative agreement with the National Science Foundation.

³The WIYN Observatory is a joint facility of the University of Wisconsin-Madison, Indiana University, Yale University, and the National Optical Astronomy Observatory.

Subject headings: galaxies: ISM — quasars: absorption lines

1. Introduction

By providing a huge spectroscopic quasar database, the Sloan Digital Sky Survey (SDSS) has spurred a renewed interest in large quasar absorption-line surveys (e.g., Reichard et al. 2003; Nestor, Turnshek, & Rao 2005, hereafter NTR05; Prochaska, Herbert-Fort, & Wolfe 2005; Rao, Turnshek, & Nestor 2006; McDonald et al. 2006; York et al. 2006). Such surveys not only improve the statistics of quasar absorption lines (in some cases by several orders of magnitude), but their large sizes also allow for the discovery of rare systems. For example, surveys for intervening Mg II absorbers such as NTR05 and Nestor et al. (in preparation) have discovered significant numbers of rare “ultra-strong” Mg II absorption systems, having $\lambda 2796$ rest-frame equivalent widths $3 \text{ \AA} \lesssim W_0^{\lambda 2796} \lesssim 6 \text{ \AA}$. Systems of this strength are 50 to $10^{3.5}$ times more rare than those with $W_0^{\lambda 2796} = 0.3 \text{ \AA}$, which is a customary division between “weak” and “strong” Mg II absorbers. Previous spectroscopic surveys were of insufficient size to detect a very useful number of Mg II absorbers at these strengths. Therefore, ultra-strong absorbers represent a virtually unstudied phenomena.

The nature of the environments of less-strong Mg II absorbers have been the subject of many studies. Churchill, Kacprzak, & Steidel (2005) have reviewed our understanding of systems with $0.1 \text{ \AA} \lesssim W_0^{\lambda 2796} \lesssim 3 \text{ \AA}$. These absorbers are found to be associated with the halos of galaxies that span a range of morphological type, luminosity and impact parameter, but tend towards galaxies with $0.1 \lesssim L/L^* \lesssim 3$ and impact parameters $15 \text{ kpc} \lesssim b \lesssim 80 \text{ kpc}$. Recent results (e.g., Tripp & Bowen 2005) also suggest that the covering fraction for strong absorption at these impact parameters is significantly less than unity (perhaps ≈ 0.5). Moreover, Rao et al. (2006) have shown that a substantial fraction of systems with $W_0^{\lambda 2796} \gtrsim 0.5 \text{ \AA}$ are damped Ly α (DLA) absorbers, which have neutral hydrogen column densities $N(\text{HI}) \geq 2 \times 10^{20} \text{ atoms cm}^{-2}$. Rao et al. (2003 and references therein) have discussed imaging results on $z < 1$ DLA galaxies, finding that low-luminosity and/or low surface brightness dwarfs contribute substantially to this subset of strong Mg II absorbers. At least three DLAs with particularly strong ($2.5 \text{ \AA} \lesssim W_0^{\lambda 2796} \lesssim 3.0 \text{ \AA}$) Mg II absorption have been imaged: the Q0827+243 ($z_{\text{abs}} = 0.525$) absorber is associated with an $\approx L^*$ spiral at $b = 36 \text{ kpc}$ (Rao et al. 2003; Steidel et al. 2002); the Q1137+3907 absorber ($z_{\text{abs}} = 0.719$) is associated with a sub- L^* star-forming galaxy at $b = 18 \text{ kpc}$ and one or two possible sub- L^* neighbors (Lacy et al. 2003); and the Q1209+107 absorber ($z_{\text{abs}} = 0.630$) has a galaxy in the field that is $\approx 2L^*$ at $b = 11 \text{ kpc}$ (Le Brun et al. 1997), assuming it is at the absorber redshift.

For strong and at least partially saturated absorption lines, rest equivalent widths (REWs) give an approximate indication of the projected velocity spread, ΔV_{REW} , of the absorbing gas, with completely black saturated $\lambda 2796$ lines providing a lower-limit of $\Delta V_{REW} = 107.2 \times W_0^{\lambda 2796} \text{ km s}^{-1}$. Thus, ultra-strong Mg II absorbers exhibit strong/saturated absorption over a (lower-limit) projected velocity spread of $\Delta V_{REW} \approx 320 - 640 \text{ km s}^{-1}$. This is significantly larger than the kinematic spread seen in Galactic Mg II absorbers in quasar spectra, which have a projected velocity extent along a sightline of $125 \pm 35 \text{ km s}^{-1}$ (Savage et al. 2000).

Though few individual ultra-strong absorbers have been studied in detail, some of their properties are known. Zibetti et al. (submitted to ApJ) demonstrate that stronger absorbers are on average bluer and at smaller impact parameter. Ménard et al. (in preparation) show that the amount of reddening of the background quasar by the absorber is strongly correlated with REW, and Nestor et al. (2003) and Turnshek et al. (2005) demonstrate that the gas-phase metallicity and depletion of refractory elements in Mg II absorbers are strongly correlated with $W_0^{\lambda 2796}$. Thus, these systems are, on average, relatively metal-rich and dusty compared to weaker absorbers. Indeed, the most metal-rich known DLA absorbers all have $2 \text{ \AA} \lesssim W_0^{\lambda 2796} \lesssim 3 \text{ \AA}$. However, the results of Rao et al. (2006) and NTR05 indicate that, while it is likely that a large fraction of ultra-strong Mg II absorption systems (perhaps $\gtrsim 60\%$) have neutral hydrogen column densities above the DLA threshold of $N(\text{H I}) \geq 10^{20.3} \text{ atoms cm}^{-2}$, most (perhaps $\approx 90\%$) DLAs have $W_0^{\lambda 2796} \lesssim 3 \text{ \AA}$. It is therefore of interest to compare the range of galaxy types associated with these two overlapping classes of absorption system.

Aside from the clear empirical connection to DLA absorbers, other authors have speculated on the nature of the strongest Mg II absorbers. As a possible explanation for Mg II systems with $0.9 \text{ \AA} \lesssim W_0^{\lambda 2796} \lesssim 1.3 \text{ \AA}$ that exhibit “double-trough” absorption profiles in higher resolution data, Churchill et al. (2000) investigated the probability of a line of sight passing through galaxy pairs such as the Milky Way and either the LMC or SMC. In this regard, if the strongest absorbers do indeed trace interacting pairs, their incidence and properties could have important impact on our understanding of hierarchical formation scenarios. In addition, Bond et al. (2001) investigated the possibility that galactic superwinds give rise to sets of absorbers with $1.8 \text{ \AA} \lesssim W_0^{\lambda 2796} \lesssim 2.8 \text{ \AA}$. Confirmation of this connection would provide an important tool for the study of the evolution of global star formation and star-forming galaxies. Nestor, Turnshek, & Rao (2006) discuss evidence in support of both superwinds and interactions as possible mechanisms causing ultra-strong Mg II absorbers. Both of these connections would also have potentially important impact on the understanding of environmental effects such as the distribution of metals into the IGM (e.g., through galactic fountains).

While there are many examples of the association between less-strong Mg II absorption and galaxies with small impact parameters, the sightlines do not in general pass through the optically luminous extent of the galaxies. The simplest possible explanation for ultra-strong Mg II absorbers may therefore be that these systems select sightlines passing through the inner regions of the disks as well as the halos of massive galaxies. However, even if this is indeed the case, the processes responsible for the very large kinematic spreads would still require explanation.

Thus, depending on the nature of ultra-strong Mg II absorbers, they may have important implications for our understanding of DLA galaxies, massive galaxies, galaxy clustering, major and minor mergers, the evolution of starburst galaxies, and metals in the IGM. It is clearly of interest to determine the physical processes responsible for these rare and extreme systems with strong low-ion gas absorption over such a large interval of rest-frame velocity. Consequently, in order to constrain the nature of ultra-strong Mg II absorbers, we have initiated a program to study the associated galaxies and environments through optical imaging. Targeted follow-up spectroscopy of individual galaxies in the fields should follow. Here we present WIYN r' or i' images of the fields towards 15 quasars exhibiting Mg II absorbers with $2.69 \text{ \AA} < W_0^{\lambda 2796} \lesssim 5.97 \text{ \AA}$ and $0.42 \leq z_{abs} \leq 0.84$, and we discuss the properties of the sample of detected galaxies. We describe our observations in § 2, the results in § 3, discuss the implications of this work in § 4, and present our conclusions in § 5.

2. Observations

We conducted observations at the WIYN telescope on Kitt Peak, Arizona, using the WIYN Tip-Tilt Module and the SDSS r' and i' filters. We imaged quasar fields containing strong and ultra-strong Mg II absorbers detected in SDSS quasar spectra. For the eight absorbers with $0.42 < z_{abs} < 0.6$ we used the r' filter, and for the seven absorbers with $0.6 < z_{abs} < 0.84$ we used the i' filter to ensure that the 4000 \AA break was not redshifted into the filter bandpass. We were awarded two nights each in February of 2005 and January of 2006, although one and a half nights were lost to weather, and one night had rather poor seeing. The final night, however, had fair to good seeing throughout. In all, we were able to obtain usable images of 15 fields, though as indicated below the seeing quality was quite heterogeneous. We obtained at least three images of each field in order to facilitate removal of cosmic rays, and total exposure times were between 60 and 100 minutes per field. The quasar point spread function (PSF) was well behaved in most of our images, and bright, unsaturated stars allowed for the modelling and removal of the quasar PSF in all but two cases.

3. Results

We used the software package SExtractor (Bertin & Arnouts, 1996) to detect, deblend, and measure sources in each of our fields. All regions having at least 15 contiguous pixels with fluxes 1.5σ above the background were extracted. We calibrated our photometry using SDSS imaging results on available bright objects in each field. In Table 1 we list all resolved objects detected within an impact parameter of $b \leq 200$ kpc of the quasar sightlines under the assumption that the objects are at the absorption redshift. Uncertainties in the magnitudes were generally $\sigma_m < 0.1$ mag, resulting in better than 10% photometric accuracy. All cosmology-dependent quantities are computed assuming $\Omega_M = 0.3$, $\Omega_\Lambda = 0.7$, and $h = 0.7$. Absolute magnitudes (and luminosities) for our detections were determined using three different k -corrections⁴ for galaxy types Sc, Sa, and E. Galaxy impact parameter, b , and sizes are also given in Table 1. The apparent projected optical extents (i.e., the luminous “sizes” of galaxies) are listed as the major-axis \times minor-axis of the SExtractor-fitted ellipse, which corresponds to the source’s approximate isophotal limit. We note that the ellipses drawn on each image in Figures 2-16 are the photometric integration limits and correspond to twice the isophotal limit.

For ease of discussion, as well as to facilitate comparison of absolute magnitudes independent of filter, we also list luminosities relative to those for the “characteristic” absolute magnitudes, M^* , from Schechter function fits to the galaxy luminosity function (LF). Whereas the actual calculated value of M^* (or L^*) is correlated with the calculated faint-end slope of the LF, and varies from study to study (see table 1 of Brown et al., 2001, for example), we stress that the physically meaningful quantities are the relative number-densities of galaxies as a function of luminosity, which do not depend on the actual value of M^* . For our purposes, we adopt values for M^* determined from the SDSS for the relatively local universe (i.e., $0.02 < z < 0.22$) from Blanton et al., 2003. In our cosmology, these correspond to $M_r^* = -21.21$ and $M_i^* = -21.59$. We note that these values are for SDSS filters k -corrected to $z = 0.1$, making them perhaps non-ideal for direct comparison. However, these values have the advantages of being calculated from the same data set to which we have calibrated our photometry and, more importantly, have very similar number-densities (i.e., $\phi(M_r^*) \simeq \phi(M_i^*)$) which allows for meaningful comparisons between our two filters. Furthermore, the value for M_r^* matches that used in at least some previous work (e.g., Rao et al., 2003). Unless otherwise stated, L^* corresponds to these values throughout this work. For comparison, in the extremely local ($10h^{-1}$ Mpc $< d < 150h^{-1}$ Mpc) universe, Blanton et

⁴Computed using the IRAF package COSMOPACK, developed by Balcells & Cristobal, http://www.iac.es/galeria/balcells/publ_mbc.html.

al., 2005 find M_r^* and M_i^* to be approximately 36% and 47% fainter than the above values, respectively.

3.1. Discussion of Individual Fields

The Mg II absorption region of each spectrum is shown in Figure 1. Note that the SDSS spectra reach a minimum Mg II redshift of $z_{abs} = 0.36$. Thus, there is no absorption information available below this redshift. Above this value, the signal to noise ratios of the spectra were such that our formal $W_0^{\lambda 2796}$ detection threshold was typically between 0.4 Å and 1 Å, though for $0.36 \leq z \lesssim 0.5$ this value typically rises to between 0.6 Å and 2 Å due to increased noise at the blue end of the spectral coverage. Figures 2 through 16 show our WIYN images. All are centered on the quasar sightlines and oriented such that north is to the top and east is to the left. They are sized so that they span $420 \text{ kpc} \times 420 \text{ kpc}$ at the absorption redshift. The location of each sightline is marked with a “x” and unresolved objects classified as stars are labelled with an “s”. In all but two cases (Q0800+2150 and Q0902+3722) the Point Spread Function (PSF) was determined well enough from stars in the field that it was subtracted at the quasar position (hence the quasar appears to disappear in 13 of the 15 fields). Magnitudes and colors from the SDSS, when quoted, use the so-called SDSS “model” magnitudes⁵. For convenience, quasar names are specified as coordinate designations relative to equinox 2000, but the formal SDSS quasar names are also listed in the text.

In our discussion of each field we emphasise what we consider to be the most likely interpretation, keeping in mind that ultra-strong Mg II absorbers are rare and may select correspondingly rare galaxy types and/or environments. Due to our lack of confirmed redshifts for almost all of the galaxies in these fields, all of these interpretations should be considered preliminary. However, in many cases there is clearly good circumstantial evidence for our proposed interpretation.

3.1.1. Q0013+1414

The spectrum of Q0013+1414 (SDSS J001335.75+141424.1, $z_{em} = 1.541$) contains a strong ($W_0^{\lambda 2796} = 2.69 \pm 0.14 \text{ Å}$) Mg II absorber at $z_{abs} = 0.4838$. No other low redshift ($z \lesssim 1$) Mg II absorber was detected in the spectrum. Our WIYN r' -band image of the

⁵See <http://cas.sdss.org/dr5/en/help/docs/glossary.asp>.

field is shown in Figure 2. The seeing was poor during the observation ($\text{FWHM} \approx 1.3''$) and we reached a limiting surface brightness of $r' = 24.18 \text{ mag arcsec}^{-2}$. The galaxy $7''$ to the northeast of the sightline has $r' = 19.68$. At the absorption redshift our photometry corresponds to $L_r = 4.4/5.6/6.4 L_r^*$ (for Sc/Sa/E-type k -corrections), an impact parameter of $b = 44 \text{ kpc}$, and a projected optical extent of $\approx 50 \times 35 \text{ kpc}$. It is also detected in the SDSS images with $r' \approx 19.5$ and $g' - r' \approx 0.6$. If at $z = z_{abs}$, its blue colors would be indicative of a starbursting galaxy. We were able to obtain a very good quasar PSF subtraction and resolved light blended with the quasar PSF was also detected. We measured this residual light to have $r' \approx 22.0$, which corresponds to $0.5/0.7/0.8 L_r^*$ and $b = 16 \text{ kpc}$. The most likely interpretation is that the low impact parameter fainter source is associated with the absorption and the brighter galaxy is in the foreground. However, it is also possible that the bright galaxy is at $z = z_{abs}$ with, perhaps, the fainter galaxy as a satellite.

3.1.2. Q0232–0811

The spectrum of Q0232–0811 (SDSS J023234.06–081126.5, $z_{em} = 1.656$) contains an ultra-strong ($W_0^{\lambda 2796} = 3.69 \pm 0.28 \text{ \AA}$) Mg II absorber at $z_{abs} = 0.4523$. No other low redshift Mg II absorption system was detected. The profiles of both lines of the Mg II doublet, $\lambda 2796$ and $\lambda 2803$, appear to exhibit wings $\approx 340 \text{ km s}^{-1}$ blueward of the main absorption. Figure 3 shows an r' -band image of the field obtained under fair seeing conditions ($\text{FWHM} = 0.69''$) with a limiting surface brightness of $r' = 24.59 \text{ mag arcsec}^{-2}$. We were able to remove the quasar PSF fairly well with only moderate residuals. This revealed a source that had been blended with the quasar PSF, having $r' \approx 22.1$ and $b \approx 0.8''$, which corresponds to $L_r \approx 0.4/0.5/0.6 L_r^*$ and $b \approx 5 \text{ kpc}$. The object $7''$ to the south of the sightline is unresolved and is likely a star. The galaxy $9''$ to the south has $r' = 21.4$, which corresponds to $b = 52 \text{ kpc}$ and $L_r = 0.8/1.0/1.1 L_r^*$. It is also detected in the SDSS with $r' \approx 21.3$ and $g' - r' \approx 1.4$, which is consistent with the colors of a local late-type galaxy shifted to $z = z_{abs}$. The presence of a source essentially covering the sightline indicates that it is likely responsible for the ultra-strong absorption.

3.1.3. Q0240–0812

The spectrum of Q0240–0812 (SDSS J024008.21–081223.4, $z_{em} = 2.231$) contains a strong ($W_0^{\lambda 2796} = 2.91 \pm 0.26 \text{ \AA}$) Mg II absorber at $z_{abs} = 0.5314$. No other low redshift Mg II absorber was detected. We obtained three WIYN r' -band images. However, only one had decent seeing ($\text{FWHM} = 0.69''$), while the others were obtained in poorer conditions

(FWHM $\approx 1.3''$). The combined images reach a limiting surface brightness of $r' = 24.50$ mag arcsec $^{-2}$ to within $b \simeq 11.7$ kpc. In Figure 4 we show just the best image, with the quasar PSF removed. This image reaches $r' = 23.71$ mag arcsec $^{-2}$. The galaxy 3'' to the east has $r' = 20.96$, which corresponds to $b = 18$ kpc and $L_r = 1.7/2.3/2.8L_r^*$. It is also detected in the SDSS images with $r' \approx 21.6$ and $g' - r' \approx 0.7$, which is rather blue for being at the absorption redshift, though we note that the SDSS magnitudes might be less accurate due to the brighter limiting surface brightness and blending with the quasar PSF. We consider it highly likely that it is associated with the strong absorption.

3.1.4. Q0747+3054

The spectrum of Q0747+3054 (SDSS J074707.62+305415, $z_{em} = 0.974$) contains an ultra-strong ($W_0^{\lambda 2796} = 3.63 \pm 0.06$ Å) Mg II absorber at $z_{abs} = 0.7650$. There is also weaker Mg II absorption detected at slightly lower redshift, with $z_{abs} = 0.7219$ and $W_0^{\lambda 2796} = 0.50 \pm 0.06$, which corresponds to a velocity difference of ≈ 7400 km s $^{-1}$ from the ultra-strong absorber. There were no other low redshift Mg II absorption systems detected in the spectrum above our formal $W_0^{\lambda 2796}$ limits, though visual inspection reveals possible Mg II absorption near $\lambda \approx 4300$ Å (with $z_{abs} = 0.534$ and $W_0^{\lambda 2796} \approx 0.4$ Å). Alternatively, it may be due to Ca II (with $z_{abs} = 0.090$ and $W_0^{\lambda 3935} \approx 0.5$ Å). Our i' -band image of the field is shown in Figure 5. The seeing was fairly good (FWHM = $0.47''$) and we reach a limiting surface brightness of $i' = 24.57$ mag arcsec $^{-2}$ to within $\approx 1.5''$ of the sightline, corresponding to ≈ 11 kpc at $z = z_{abs}$. Subtraction of the quasar PSF reveals no evidence for objects down to $\approx 0.8''$, or $b = 6$ kpc. The two brightest objects in the field are also detected in the SDSS images; the galaxy 5'' (38 kpc at $z = z_{abs}$) to the northwest with $i' \approx 19.5$ and $g' - i' \approx 2.1$ (consistent with the colors of a local late-type galaxy shifted to $z = z_{abs}$), and the galaxy 9'' (63 kpc at $z = z_{abs}$) to the northeast with $i' \approx 20.9$ and $g' - i' \approx 3$ (consistent with the colors of a local intermediate-type galaxy shifted to $z = z_{abs}$). Also, a visual inspection of Figure 5 is suggestive of one or more galaxy groups to the north and west.

Due to the wealth of objects detected in the image and the multiple absorbers seen in the quasar spectrum, interpretation of results for the ultra-strong Mg II absorber in this field is difficult. Further complicating the situation is the relatively low redshift of the quasar – there is a possibility that some of the detected sources are in a group that includes the quasar host at $z \approx 0.97$. There are several reasonable explanations for the presence of the ultra-strong absorber. One or more of the bright galaxies could be associated with the ultra-strong absorber. Although galaxies this bright are rare, so are absorbers of this strength. Alternatively, if the bright galaxies are in the foreground, the ultra-strong absorber could be

associated with a galaxy group consisting of several of the other detected sources. Finally, it is possible that one of the fainter sources is a field galaxy at the redshift of the ultra-strong absorber. Spectroscopy of this field would be particularly helpful for understanding this intriguing system.

3.1.5. Q0747+3354

The spectrum of Q0747+3354 (SDSS J074758.65+335432.5, $z_{em} = 1.700$) contains an ultra-strong ($W_0^{\lambda 2796} = 4.69 \pm 0.25 \text{ \AA}$) Mg II absorber at $z_{abs} = 0.6202$. No other low redshift Mg II absorption system was detected. Our i' -band image is shown in Figure 6. The seeing was poor (FWHM = $1.2''$), but we were able to obtain an excellent subtraction of the quasar PSF. We reach a limiting surface brightness of $i' = 24.30 \text{ mag arcsec}^{-2}$. The object to the west is unresolved. The galaxy $2''$ to the east has $i' = 21.11$, corresponding to $b = 12.8 \text{ kpc}$ and $1.4/1.7/2.0 L_i^*$. The galaxy $5''$ to the northeast has $i' = 23.14$, which corresponds to $b = 34 \text{ kpc}$ and $0.2/0.3/0.3 L_i^*$. Neither are detected in the SDSS images. It is likely that at least one of these galaxies is associated with the absorber.

3.1.6. Q0800+2150

The spectrum of Q0800+2150 (SDSS J080005.3+215015.2, $z_{em} = 1.790$) contains an ultra-strong ($W_0^{\lambda 2796} = 3.65 \pm 0.16 \text{ \AA}$) Mg II absorber at $z_{abs} = 0.5716$. There is also strong Mg II absorption in the spectrum at higher redshift ($z = 0.994$ and $z = 1.181$). Our r' -band image obtained under fair seeing conditions (FWHM = $0.54''$) is shown in Figure 7. We reach a limiting surface brightness of $r' = 25.14 \text{ mag arcsec}^{-2}$ to within $\approx 1.6''$ of the sightline, corresponding to $\approx 10 \text{ kpc}$ at $z = 0.5716$. There was not a sufficient number of bright unsaturated stars in the field to subtract the quasar PSF. We detect six resolved objects within $b = 100 \text{ kpc}$ of the sightline, none of which were detected in the SDSS images. The two detections with the lowest impact parameters ($3''$, or $b = 19 \text{ kpc}$) to the northeast and southeast have $r' = 22.22$ and $r' = 24.63$, respectively, corresponding $0.7/1.0/1.2 L_r^*$ and $0.1/0.1/0.1 L_r^*$, respectively. It is likely that at least one of these is associated with the ultra-strong absorber.

3.1.7. Q0836+5132

The spectrum of Q0836+5132 (SDSS J083618.76+513244.1, $z_{em} = 1.550$) contains an ultra-strong ($W_0^{\lambda 2796} = 3.48 \pm 0.21 \text{ \AA}$) Mg II absorber at $z_{abs} = 0.5666$. No other low redshift Mg II absorption system was detected. We obtained an r' -band image under poor seeing conditions (FWHM= $1.6''$), but were able to model and remove the quasar PSF with only moderate residuals (see Figure 8.) We reach a limiting surface brightness of $r' = 25.32 \text{ mag arcsec}^{-2}$. The PSF subtraction reveals a galaxy $2''$ to the south of the sightline with $r' \approx 23.1$, which corresponds to $b = 10 \text{ kpc}$ and $0.3/0.4/0.5 L_r^*$. It is not detected in the SDSS images. The large, bright galaxy $26''$ to the southwest has an SDSS spectroscopic redshift of $z = 0.113$. It is likely that the faint, low impact parameter galaxy is associated with the ultra-strong absorber.

3.1.8. Q0902+3722

The spectrum of Q0902+3722 (SDSS J090212.76+372208, $z_{em} = 1.242$) contains an ultra-strong ($W_0^{\lambda 2796} = 3.97 \pm 0.18 \text{ \AA}$) Mg II absorber at $z_{abs} = 0.6700$. Weaker absorption is also detected at $z_{abs} = 0.932$ and $z_{abs} = 1.121$ with $W_0^{\lambda 2796} = 1.1 \text{ \AA}$ and $W_0^{\lambda 2796} = 0.3 \text{ \AA}$, respectively. We obtained an i' -band image of the field under moderate seeing conditions (FWHM= $0.61''$) that reaches a limiting surface brightness of $i' = 24.20 \text{ mag arcsec}^{-2}$ down to within $\approx 1.35''$ of the sightline, corresponding to $b = 9.5 \text{ kpc}$ (Figure 9). Due to strong residuals, removal of the quasar PSF did not improve the minimum searchable impact parameter. We detect three resolved sources near the sightline, none of which are cataloged in the SDSS. The galaxies $3''$ and $5''$ to the southeast have $i' = 21.42$, and $i' = 21.70$, respectively, corresponding to $b = 18 \text{ kpc}$ and $1.3/1.6/1.9 L_i^*$ and $b = 37 \text{ kpc}$ and $1.0/1.3/1.5 L_i^*$, respectively. The galaxy $5''$ to the northwest has $i' = 22.38$ corresponding to $b = 36 \text{ kpc}$ and $0.6/0.7/0.8 L_i^*$. At least one of these galaxies is likely to be associated with the ultra-strong absorber. The irregular appearance of the galaxy further to the southeast suggests it is interacting with either a satellite or the other galaxy to the southeast of the sightline.

3.1.9. Q1000+4438

The spectrum of Q1000+4438 (SDSS J100015.51+443848, $z_{em} = 1.862$) contains an ultra-strong ($W_0^{\lambda 2796} = 5.33 \pm 0.19 \text{ \AA}$) Mg II absorber at $z_{abs} = 0.7192$. There is also Mg II absorption at $z_{abs} = 0.6964$ with $W_0^{\lambda 2796} = 1.21 \pm 0.12 \text{ \AA}$, which is a velocity difference of $\approx 4000 \text{ km s}^{-1}$ from the ultra-strong absorption. We obtained an i' -band image of the field

with seeing FWHM = $0.93''$ that reaches a limiting surface brightness of $i' = 24.72$ mag arcsec $^{-2}$. We were able to model and remove the quasar PSF with only mild residuals, revealing a $i' \approx 21.5$ magnitude source $1''$ from the sightline that was blended with the light from the quasar (see Figure 10). This corresponds to $b = 8$ kpc and $1.5/1.9/2.2 L_i^*$. It is not detected in the SDSS data. Also detected in our image is a fainter galaxy $6''$ to the northeast with $i' = 23.94$, which corresponds to $b = 44.3$ kpc and $0.2/0.2/0.3 L_i^*$. It is likely that one of these galaxies is associated with the ultra-strong absorber, while the other is associated with the weaker, $z_{abs} = 0.6964$ absorber. Alternatively, they may be a pair, and the galaxy associated with one of the two absorbers is either not detected or associated with one of the larger impact parameter galaxies in the field.

3.1.10. Q1011+4451

The spectrum of Q1011+4451 (SDSS J101142.01+445155.4, $z_{em} = 1.919$) contains an ultra-strong ($W_0^{\lambda 2796} = 4.94 \pm 0.15 \text{ \AA}$) Mg II absorber at $z_{abs} = 0.8360$. There is also relatively strong Mg II absorption with $W_0^{\lambda 2796} = 1.6 \text{ \AA}$ at $z_{abs} = 0.675$. We obtained an i' -band image (Figure 11) with a seeing of FWHM = $0.56''$ and were able to remove the quasar PSF with moderate residuals (masked out in Figure 11). We reach a limiting surface brightness of $i' = 24.60$ mag arcsec $^{-2}$. There are two bright, low impact parameter galaxies detected in the field. The galaxy $4''$ to the south has $i' = 20.63$, corresponding to $b = 32$ kpc, $5.3/7.4/9.2 L_i^*$, and a projected optical extent of $\approx 27 \times 22$ kpc. It is classified as a star in the SDSS with $i' \approx 21.1$ and $g' - i' \approx 4$ (though we note that it is only marginally detected in the SDSS data), which is consistent with the colors of a local early-type galaxy shifted to $z = z_{abs}$. The galaxy $6''$ to the west has $i' = 21.10$, corresponding to $b = 45$ kpc, $3.6/5.0/6.2 L_i^*$, and a projected optical extent of $\approx 30 \times 24$ kpc. It is detected in the SDSS images with $i' \approx 21.4$ and $g' - i' \approx 1.6$, which is consistent with the colors of a local late-type/starburst galaxy shifted to $z = z_{abs}$. We also detect fainter galaxies $3''$ to the north and $6''$ to the northwest with $i' = 24.45$ and $i' = 24.10$, respectively, corresponding to $b = 20$ kpc and $0.2/0.2/0.3 L_i^*$ and $b = 46$ kpc and $0.2/0.3/0.4 L_i^*$, respectively. There are also three other faint galaxies with $50 < b < 100$ kpc and $L < L_i^*$. It is probable that at least one and perhaps several of the detected galaxies are at the redshifts of the ultra-strong and strong absorbers. However, it would seem that no unique interpretation is significantly more likely than the alternatives.

3.1.11. Q1038+4727

The spectrum of Q1038+4727 (SDSS J103808.67+472734.9, $z_{em} = 1.047$) contains an ultra-strong ($W_0^{\lambda 2796} = 3.14 \pm 0.08 \text{ \AA}$) Mg II absorber at $z_{abs} = 0.5292$. No other low redshift Mg II absorption system was detected. We obtained an r' -band image (Figure 12) with seeing FWHM=0.82'', reaching a limiting surface brightness of $r' = 24.35 \text{ mag arcsec}^{-2}$, and were able to remove the quasar PSF with moderate residuals (masked out in the image). The galaxy 2'' to the northwest has $r' = 21.12$, which corresponds to $b = 15 \text{ kpc}$ and $1.5/2.1/2.4 L_r^*$. It is not cataloged by the SDSS. There is also a fainter source detected further to the northwest ($b = 35 \text{ kpc}$). We consider it likely that the low impact parameter galaxy is at the redshift of the absorber, and perhaps part of a pair with the fainter galaxy.

3.1.12. Q1356+6119

The spectrum of Q1356+6119 (SDSS J135603.78+611949.6, $z_{em} = 1.873$) contains an ultra-strong ($W_0^{\lambda 2796} = 5.97 \pm 0.34 \text{ \AA}$) Mg II absorber at $z_{abs} = 0.7850$. No other low redshift Mg II absorber was detected. We obtained an i' -band image (Figure 13) under moderate seeing conditions (FWHM=0.66'') and were able to remove the quasar PSF with moderate residuals. We reach a limiting surface brightness of $i' = 24.48 \text{ mag arcsec}^{-2}$. The galaxy 1'' to the northwest has $i' \approx 21.7$, which corresponds to $b = 9 \text{ kpc}$ and $1.7/2.2/2.7 L_i^*$. It is likely that this galaxy is associated with the ultra-strong absorption. There are also three galaxies to the north with $50 \text{ kpc} < b < 80 \text{ kpc}$ and $0.5L^* < L(z = z_{abs}) < 1.5L^*$ that could potentially form a group at $z = z_{abs}$. None of the low impact parameter galaxies is detected in the SDSS images. Additionally, there may be a large group farther to the north and west. The presence of several bright ($i' < 20$) galaxies suggest that they are most likely in the foreground, but it cannot be ruled out that they are at $z \approx z_{abs}$.

3.1.13. Q1417+0115

The spectrum of Q1417+0115 (SDSS J141751.84+011556.1, $z_{em} = 1.727$) contains an ultra-strong ($W_0^{\lambda 2796} = 5.6 \pm 0.5 \text{ \AA}$) Mg II absorber at $z_{abs} = 0.6689$. No other low redshift Mg II absorber was detected. We obtained an i' -band image (Figure 14) under poor seeing conditions (FWHM=1.2''). The PSF in the image was asymmetric due to wind-shake and the process of removing the quasar PSF was somewhat uncertain, leaving strong residuals (masked out in Figure 14) within $r = 10 \text{ pixels}$ ($b = 7.9 \text{ kpc}$). We reach a limiting surface brightness of $i' = 23.90 \text{ mag arcsec}^{-2}$. There are two relatively bright galaxies within 100

kpc of the sightline. The galaxy 9'' to the northeast has $i' = 20.33$, which corresponds to $b = 60$ kpc, $3.6/4.4/5.2 L_i^*$, and a projected optical extent of $\approx 27 \times 25$ kpc. It is classified as a star by the SDSS with $i' \approx 20.6$ and $g' - i' \approx 1.5$; however, the colors are consistent with those of a local late-type/starburst galaxy shifted to $z = z_{abs}$. The galaxy 12'' to the southeast has $i' = 19.32$, which corresponds to $b = 86$ kpc, $9.1/11.0/13.2 L_i^*$, and a projected optical extent of $\approx 42 \times 38$ kpc. It is detected in the SDSS images with $i' \approx 18.9$ and $g' - i' \approx 2.4$, which is consistent with the colors of a local intermediate/late-type galaxy shifted to $z = z_{abs}$. There are also fainter resolved sources detected in our image including a low impact parameter galaxy 4'' ($b = 29$ kpc) to the southwest with $i' = 21.86$ ($0.8/1.0/1.2 L_i^*$). This low impact parameter galaxy may be associated with the ultra-strong absorption, while the bright galaxies are in the foreground. However, it is possible that the bright galaxies are indeed (also) at $z = z_{abs}$, and are part of a group or exhibit superwinds, accounting for the ultra-strong $W_0^{\lambda 2796}$ of this absorber.

3.1.14. Q1427+5325

The spectrum of Q1427+5325 (SDSS J142749.37+532508.9, $z_{em} = 0.909$) contains an ultra-strong ($W_0^{\lambda 2796} = 4.35 \pm 0.17 \text{ \AA}$) Mg II absorber at $z_{abs} = 0.5537$. No other low redshift Mg II absorber was detected. We obtained an r' -band image (Figure 15) under poor seeing conditions (FWHM=1.1''). We were able to remove the quasar PSF, but with moderately strong residuals. We reach a limiting surface brightness of $r' = 24.81$ mag arcsec⁻². There appear to be three separate sources blended with the quasar PSF, although the poor seeing and residuals make it difficult to determine if they are in fact separate sources or if some of them are the same object. They are not cataloged in the SDSS. If at $z = z_{abs}$ they would total $L \approx 3-4L^*$ within $b \leq 35$ kpc. There are also several additional galaxies with impact parameters and luminosities in the range $35 \text{ kpc} < b < 95 \text{ kpc}$ and $0.1L_r^* \lesssim L(z = z_{abs}) \lesssim 1.5L^*$. We consider it very likely that the galaxy (or galaxies) surrounding the sightline are associated with the ultra-strong absorption, possibly forming part of a larger group with the other nearby galaxies. We also note, however, that due to the relatively low redshift of the quasar it is possible that we are detecting some light from the quasar host as well.

3.1.15. Q1520+6105

The spectrum of Q1520+6105 (SDSS J152046.36+610511.3, $z_{em} = 2.182$) contains an ultra-strong ($W_0^{\lambda 2796} = 4.24 \pm 0.14 \text{ \AA}$) Mg II absorber at $z_{abs} = 0.4235$. No other low redshift

Mg II absorber was detected. We obtained an r' -band image (Figure 16) in fair seeing conditions (FWHM=0.76'') and were able to remove the quasar PSF. We reach a limiting surface brightness of $r' = 24.03$ mag arcsec $^{-2}$. The galaxy 4'' northwest of the sightline has $r' = 19.72$, which corresponds to $b = 20$ kpc and $2.9/3.5/3.9 L_r^*$. It is the only source that we detect within $b \leq 80$ kpc of the sightline and consider it likely that it is physically associated with the ultra-strong absorber. It is detected in the SDSS images with $r' \approx 19.6$ and $g' - r' \approx 1.6$, which is consistent with the colors of a local intermediate/late-type galaxy shifted to $z = z_{abs}$.

3.2. Statistical Properties of the Sample

Each of the sightlines imaged in this work contains a very strong Mg II absorption system in the redshift range $0.42 < z_{abs} < 0.84$. Thus, it is expected that the fields surrounding each sightline will, on average, exhibit more sources at $z \approx z_{abs}$, in comparison to a randomly selected field. Figure 17 demonstrates this excess along our sightlines for the detected galaxies which would have $L(z = z_{abs}) \geq 0.5L^*$. There is a clear overdensity of galaxies within $b \approx 45$ kpc in comparison to larger impact parameters by a factor of ≈ 4 for $30 \text{ kpc} < b < 45 \text{ kpc}$ and rising to a factor of ≈ 10 for $b < 15$ kpc. Of course, each field is contaminated by both foreground and background sources that are physically unrelated to the absorption environment. In particular, many of the apparently bright sources may be foreground galaxies.

Our 15 fields contain a total of 13 sources that, if at $z = z_{abs}$, would have $4L^* \lesssim L \lesssim 13L^*$ and $b < 200$ kpc. More than half of these would have $b < 90$ kpc, even though this covers only $\approx 20\%$ of the area. Locally, galaxies as bright as $4L^*$ are less numerous than L^* galaxies by a factor of ≈ 25 (Blanton et al. 2003), and are almost exclusively early-type (Nakamura et al. 2003), and/or cD cluster galaxies (e.g., Laine et al. 2003), while galaxies with $L \gtrsim 8L^*$ are extremely rare, having number densities $\lesssim 10^{-3}$ times that for L^* galaxies.⁶ Thus, it is possible that some of them are in the foreground of the absorber, and consequently less luminous than the $z_{gal} = z_{abs}$ assumption implies. In order to explore whether all of the bright galaxies in our sample can be accounted for by foreground objects, we created simulated galaxy catalogs for the fields under study using the galaxy number counts in the r' and i' bands from the SDSS commissioning data (Yasuda et al. 2001). The counts in that

⁶We note, however, that bright galaxies were more common in the past. The results of Gabasch et al., 2006 suggest that $4L^*$ galaxies were more common at $0.45 < z < 0.85$ by a factor of ≈ 2.5 and $8L^*$ galaxies by a factor of ≈ 20 , compared to the Blanton et al. 2003 results.

study reliably reach at least $r' \approx i' \approx 20$. Beyond this value, we extrapolate using the faint-end of the number-magnitude curve. Subaru Deep Field data (Nagashima et al. 2002) show that the counts-magnitude relation turns over rather slowly at fainter visual magnitudes. By extrapolating from the Yasuda et al. results, we at worst slightly overpredict the expected number of galaxies at the faint end of our modeled sample, but this has no effect on the predicted number of bright galaxies.

We randomly populated each field with galaxies according to the number-magnitude relation for 100 Monte Carlo simulations. For various luminosity ranges (assuming all have $z_{gal} = z_{abs}$ and using the average of Sa- and Sc-type k -corrections) we then computed the cumulative number of galaxies within a given impact parameter for the sum of all sightlines, and we compared these results to our data. The results are shown in Figure 18. The upper-left panel shows the cumulative distribution for galaxies with $0.5L^* \leq L(z = z_{abs}) < 1L^*$. We find fewer galaxies within $b = 200$ kpc than expected from our simulation at $> 95\%$ confidence. While cosmic variance, which is not considered in our simulation, would not affect the overall average, it would expand the range of the confidence intervals, and thus this dearth could be due to cosmic variance. More likely, however, it is due to an overestimation of the number of apparently-faint galaxies in our simulation due to the inexact extrapolation of the faint end of the number-magnitude relation. Notably, there is a significant *excess* of galaxies within $b \approx 60$ kpc. The low impact parameter galaxy excess is seen more distinctly in the upper-right panel which shows the distribution for galaxies with $1L^* \leq L(z = z_{abs}) < 2L^*$. Surprisingly, although the excess is less significant for galaxies with $2L^* \leq L(z = z_{abs}) < 4L^*$, it is *very* significant for galaxies with $L(z = z_{abs}) \geq 4L^*$.

In Figure 19, we show the number of galaxies with $L \geq 0.5L^*$ as function of magnitude for two ranges of impact parameter, $10 \text{ kpc} < b < 45 \text{ kpc}$ and $90 \text{ kpc} < b < 200 \text{ kpc}$, as well as the predictions from the Monte Carlo simulations. The excess at low- b can be seen to hold over a large range of luminosity. For $b > 90$ kpc, there is good agreement between the measured galaxy number-luminosity relation and the simulations. Thus, the larger- b galaxies are consistent with being uncorrelated with the presence of the ultra-strong Mg II absorption at the level detectable by our small sample. The excess at low- b does not necessarily represent the LF of ultra-strong Mg II absorber *galaxies*, but rather the LF of all galaxies in ultra-strong Mg II absorber *environments*. However, there are 19 detected sources in this magnitude and impact-parameter range, compared to an average of 4.4 in our simulations. Although this does not include sources fainter than $0.5L^*$ or within $b \leq 10$ kpc (which total an additional 14 sources), the net average number of galaxies over the expected foreground plus background is approximately one per sightline.

To compare this excess to the LF of field galaxies at similar redshift, we also show in

Figure 19 the results of the simulation plus the r' -band LF at $0.45 < z \leq 0.85$ from Gabasch et al. (2006) renormalized (by a factor of $\simeq 40$) such that the sum matches the data in the $0.5L^* < L < 1.0L^*$ range. The shape of the LF for ultra-strong Mg II absorber environments at $0.4 \lesssim z \lesssim 0.8$ appears to be roughly consistent with that of random environments at similar redshift, with perhaps an excess of galaxies with $1L^* \leq L < 2L^*$ relative to slightly fainter and slightly brighter galaxies. Larger samples are necessary to confirm/quantify this. Additionally, even though bright galaxies were more common in this redshift range than at $z = 0$, the expected number of $L > 4L^*$ galaxies with $10 \text{ kpc} < b < 45 \text{ kpc}$ from the sum of the Monte Carlo simulations plus the $0.45 < z \leq 0.85$ LF is only $\langle n_{gal} \rangle \simeq 1$, whereas we detected four.

The excess of galaxies with $4L^* \leq L(z = z_{abs}) < 13L^*$ seen in Figures 18 and 19 is unlikely to be due to cosmic variance. While a chance low redshift galaxy group along one of our sightlines could produce an apparent excess, we note that the putative $4L^* \leq L < 13L^*$ galaxies are distributed among several fields, making the idea of appealing to some kind of foreground effect less likely. In our data, the seven galaxies with $4L^* \leq L(z = z_{abs}) < 13L^*$ and $b < 90 \text{ kpc}$ are distributed over four fields: Q0013+1414, with $L(z = z_{abs}) \approx 5L^*, b = 44 \text{ kpc}$; Q0747+3054 with $L(z = z_{abs}) \approx 12L^*, b = 38 \text{ kpc}$ and $L(z = z_{abs}) \approx 4.5L^*, b = 63 \text{ kpc}$; Q1011+4451 with $L(z = z_{abs}) \approx 6.4L^*, b = 32 \text{ kpc}$ and $L(z = z_{abs}) \approx 4L^*, b = 45 \text{ kpc}$; and Q1417+0115 with $L(z = z_{abs}) \approx 4L^*, b = 60 \text{ kpc}$ and $L(z = z_{abs}) \approx 10L^*, b = 86 \text{ kpc}$. The six $4 \leq L(z = z_{abs}) < 13L^*$ galaxies with $b > 90 \text{ kpc}$ are all in other fields, with one each towards Q0800+2150 and Q0902+3722 and four towards Q1356+6119. We also note that all of these larger impact parameter bright galaxies have $b \geq 160 \text{ kpc}$, i.e., there is a gap from $b = 86 \text{ kpc}$ to $b = 160 \text{ kpc}$ where we detect no galaxies brighter than $L(z = z_{abs}) \approx 4L^*$. Thus, while cosmic variance cannot be ruled out as the explanation for some of the bright, low impact parameter galaxies in our data, it seems likely that the bulk are at the absorption redshift and in some way related to the very large velocity spreads of the Mg II absorption along the quasar sightlines.

4. Discussion

Each of our fields contains at least one detected galaxy with $L \gtrsim 0.3L^*$ and $b \lesssim 40 \text{ kpc}$, and many have detected galaxies with optical extents blended with the quasar PSF. In studies of galaxies associated with quasar absorption lines, it is customary to simply state luminosities and impact parameters. However, when the impact parameter is small, the *size* of the galaxy is also relevant. More specifically, it is of interest to know impact parameters scaled by some measure of the luminous radii of the galaxies in the field. There-

fore, we define the radius of the optical extent of the galaxy along the direction towards the quasar, $R_{gal-quasar}$, and consider the ratio of the impact parameter b to this quantity, $\varepsilon = b/R_{gal-quasar}$. Though the measured values of $R_{gal-quasar}$ will be sensitive to the galaxy’s luminosity and redshift, as well as the seeing quality and depth of our photometry in each field, ε is nonetheless suggestive of a more physical, if approximate, indication of the region of a galaxy that is being sampled by the sightline. Using this measurement, we find that five of our fields (Q0232-0811, Q0747+3354, Q1000+4438, Q1356+6119, and Q1427+5325) have a galaxy overlapping the sightline (i.e., $\varepsilon < 1$). Two additional fields (Q0836+5132 and Q1520+6105) have detected galaxies with $\varepsilon \lesssim 1.3$. In seven of the remaining fields the closest detected galaxies have $1.5 < \varepsilon < 2.5$ and one field (Q1417+0115) has $\varepsilon \approx 4$. Many of the low impact parameter galaxies detected in our sample appear to have a fainter neighbor. We quantify this in a similar fashion as above. If a galaxy with $b < 50$ kpc has a neighbor within $\varepsilon_{gal-gal} < 2$ we consider this evidence for a “pair”. Five of our 15 sightlines meet this criterion, and another three have $2 < \varepsilon_{gal-gal} < 3$, where we list the evidence for a pair as “close.” Using this information, together with the images themselves, we can tentatively categorize each field as “normal” (i.e., similar to sightlines of less-strong Mg II absorbers, with a $0.3L^* \lesssim L \lesssim 2L^*$ galaxy at $b \lesssim 50$ kpc), “overlap” (i.e., having sightlines which intersect the optically-luminous extents of the galaxies), “interacting” (i.e., exhibiting evidence for distorted morphology or interacting galaxies), and/or “bright” (i.e., having multiple $L \gtrsim 4L^*$ galaxies with $b \leq 90$ kpc in the field.) We summarize these findings in Table 2. We also note that visual inspection of the images suggests that a cluster or a large group may be present in several of the fields, particularly Q0747+3054, Q0800+2150, and Q1356+6119.

Our four weakest systems, which have $2.7 \text{ \AA} \lesssim W_0^{\lambda 2796} \lesssim 3.5 \text{ \AA}$, are all categorized as “normal”. The seven systems with $3.6 \text{ \AA} \lesssim W_0^{\lambda 2796} \lesssim 4.7 \text{ \AA}$ are represented by all of our categories. Among the four strongest absorbers, which have $5 \text{ \AA} \lesssim W_0^{\lambda 2796} \lesssim 6 \text{ \AA}$, two are categorized as “bright” and two as “overlap”. However, we emphasize that the number of sightlines we have studied is small, and that apparent trends with $W_0^{\lambda 2796}$ may not be supported by larger samples.

Surprisingly, almost half of the images in our sample appear similar to fields selected by less-strong Mg II absorbers, i.e., in the “normal” category. Thus, we have little additional evidence to diagnose the cause of the large kinematics seen in absorption for those systems. It is therefore possible that some ultra-strong Mg II systems simply represent the tail of the distribution of galaxy kinematics and chance alignment of the sightline with many low-ionization absorbing clouds in the galaxy halo. This interpretation is consistent with the findings of Rao et al. (2006) where they find that, while the fraction of Mg II absorbers that are DLAs increases with increasing $W_0^{\lambda 2796}$, not all ultra-strong Mg II systems are DLAs.

In this picture, an increasing number of kinematically-distinct “clouds” intercepted by the sightline increases both the observed $W_0^{\lambda 2796}$ and the likelihood that at least one of the clouds exhibits a H I column density above the DLA threshold.

Five to seven of our images reveal the presence of a galaxy overlapping (or nearly so) the sightline. This raises the question of whether many ultra-strong systems might simply select sightlines through the inner regions (as opposed to the extended-halos) of normal galaxies. However, Galactic Mg II absorption seen against quasars has only a median $W_0^{\lambda 2796} = 1.17 \pm 0.33 \text{ \AA}$ (Savage et al. 2000) which corresponds to $\Delta V_{REW} = 125 \pm 35 \text{ km s}^{-1}$. These systems, of course, sample only roughly half of a complete sightline through the Galactic disk. Nonetheless, the absorption kinematics tend to be at most only slightly asymmetric about the Local Standard of Rest. To account for the asymmetry, we use the minimum/maximum velocity limits of each absorber given by Savage et al. to estimate that a full line of sight through the disk would only increase the observed absorption strengths by $\approx 10\%$ to 50% , and in no case more than $\approx 70\%$. Thus, it is not expected that the Milky Way would produce an ultra-strong Mg II absorber, even with a sightline passing through the entire disk at the solar locus. If there is a significant intermediate redshift population with smaller velocity spreads (i.e., smaller $W_0^{\lambda 2796}$ values) but having similar overlapping galaxy–sightline pairs, the discrepancy would simply be due to our observing only ultra-strong systems. The absence of this population, however, would mean that our sample is fairly representative and would imply that galaxies containing significant amounts of neutral/low-ion gas at $0.4 \lesssim z \lesssim 0.8$ were in general kinematically more complex than the Milky Way. This is consistent with the findings of NTR05 whereby the total proper cross section for absorption by ultra-strong Mg II absorbers is decreasing with decreasing redshift, especially for $z \lesssim 1$, indicating a larger incidence of ultra-strong systems at intermediate redshift compared to the present epoch. We also note that this difference is consistent with the decreasing global star formation rate from $z \approx 1$, which may be relevant if the kinematics are driven by star formation.

Using HST ACS images, Kacprzak, Churchill, & Steidel (2005) have argued that, for systems with $0.03 \text{ \AA} \lesssim W_0^{\lambda 2796} \lesssim 1.2 \text{ \AA}$, the absorption-line kinematics are correlated with galaxy asymmetry divided by impact parameter. Of course, our $W_0^{\lambda 2796}$ values are significantly larger and we cannot produce their asymmetry measurements for our sample with ground-based data; however, it is interesting that at least a third of our sample shows evidence for a low impact parameter pair. Although some of these putative pairs are likely foreground or background coincidences, the presence of an interacting pair could provide the kinematic complexity necessary for the presence of an ultra-strong Mg II absorber.

In addition, the evidence for $4L^* \lesssim L \lesssim 13L^*$ galaxies with $b \leq 90 \text{ kpc}$ has interesting

consequences. If these galaxies are confirmed to be starburst galaxies at $0.42 \lesssim z \lesssim 0.84$, they would represent an intermediate stage between the high redshift starburst population (i.e., Lyman-break galaxies), which exhibit a characteristic rest frame optical luminosity $L_{LBG}^* \simeq 6-9L^*$ (Shapley et al. 2001) and can reach $L \gtrsim 20L^*$, and local starbursts which are generally compact (e.g., Brinchmann et al. 2004) with typical luminosities $L \lesssim 1-2L^*$ (Meurer et al. 2006). The connection between strong, low-ionization absorption and outflows from starburst galaxies has already been established. Schwartz et al. (2006), for example, find C II absorption with $1 \text{ \AA} \lesssim W_0^{\lambda 1335} \lesssim 5.6 \text{ \AA}$ and $350 \text{ km s}^{-1} \lesssim \text{FWHM} \lesssim 1400 \text{ km s}^{-1}$ in outflows from individual star clusters in nearby UV-selected galaxies. Pettini et al. (2002) find low-ion (e.g., C II $\lambda 1334$, Si II $\lambda 1526$, Al II $\lambda 1670$, Fe II $\lambda 2344$) absorption with REWs $\simeq 2.6\text{\AA} - 3.5\text{\AA}$ in the spectrum of the $z = 2.7$ gravitationally lensed LBG MS 1512–cB58, and Shapley et al. (2003) find stacked spectra of $z \sim 3$ LBGs to have average C II $\lambda 1334$ and Si II $\lambda 1526$ absorption $\text{FWHM} = 560 \pm 150 \text{ km s}^{-1}$. It is noteworthy that both of our strongest fields that *do not* show evidence for a source with $\varepsilon < 1$, *do* contain two $L(z = z_{abs}) \gtrsim 4L^*$ galaxies with $b \leq 90 \text{ kpc}$. Furthermore, in each of the three fields that have two such bright galaxies, the quasar sightlines are “bracketed” by the bright galaxies, i.e., the sightlines are intermediate in RA and/or DEC to the galaxies. If these galaxies in close proximity to the sightlines are undergoing massive starbursts with galactic outflows at the absorption redshift, they could easily explain the huge ΔV_{REW} seen in absorption.

Although our sample is not large and presently lacks galaxy-redshift information, it does suggest a general picture of the nature of ultra-strong Mg II absorbers. Many such systems are similar to less-strong Mg II absorbers, and may represent the tail of the kinematic distribution caused by the chance alignment of many low-ionization absorbing clouds. Some of these cases are due to the sightline passing in close proximity to, or through, the inner regions of relatively bright galaxies that, due to interactions and/or star formation, are kinematically more complex than relatively quiescent galaxies such as the Milky Way. These categories are not separate, but may loosely correlate with absorption strength. Additionally, a smaller fraction of ultra-strong systems may be due to the winds of very luminous star-forming galaxies with $4L \lesssim L^* \lesssim 13L^*$. These tend to be among the strongest systems. This proposed dual-cause scenario is suggested by the results presented in Table 2 and is consistent with the results shown in Figure 18, including the weaker excess of $L \approx 3L^*$ galaxies compared to those with $L \approx 1-2 L^*$ and $L \gtrsim 4L^*$. Of course, larger samples would be needed to constrain any real correlations; follow-up spectroscopy would greatly aid in understanding individual fields and confirming or repudiating the general picture suggested above.

5. Conclusions

We have presented optical images of the fields surrounding 15 quasars that exhibit intermediate redshift strong (two systems with $2.7 \text{ \AA} \lesssim W_0^{\lambda 2796} \lesssim 3 \text{ \AA}$) or ultra-strong (13 systems with $W_0^{\lambda 2796} \gtrsim 3 \text{ \AA}$) Mg II absorption in their spectra at redshifts $0.42 < z_{abs} < 0.84$. All of the fields reveal at least one relatively bright galaxy within an impact parameter of 40 kpc to the quasar sightline. We have demonstrated a statistical overdensity of galaxies within $b \lesssim 90$ kpc of the absorber sightlines compared to predictions for randomly selected fields, and have shown that this excess extends over a large range of luminosity. There is evidence for an excess of galaxy pairs, interactions, and very bright ($4L^* \lesssim L \lesssim 13L^*$) galaxies close to the sightlines as well. A significant number of our fields appear similar to those for less-strong systems, but many of the ultra-strong Mg II absorber sightlines pass through the apparent stellar luminous extent of relatively bright galaxies. Since these absorbers exhibit velocity spreads much larger than those expected for sightlines passing through the Milky Way, these observations indicate the existence of intermediate redshift galaxies that are more kinematically complex than the Milky Way and a method for identifying them. Interacting galaxy pairs and starburst activity may in part contribute to the very large kinematic spreads that define these systems. Finally, our results provide evidence that galactic winds from a population of bright galaxies, that are intermediate to high-redshift Lyman break galaxies and local starbursts, may contribute to the ultra-strong Mg II absorber population. It would be very helpful to obtain spectra of individual galaxies in the fields discussed in this paper, as this would eliminate many of the ambiguities in the interpretations of the individual fields.

We wish to thank the the NOAO WIYN staff as well as Michele Belfort-Mihalyi for help in acquiring our data. DBN acknowledges support from NSF grant AST-9984040. DAT and SMR acknowledge support from NSF grant AST-0307743. AMQ acknowledges REU support from NSF grant AST-0307743.

We thank members of the SDSS collaboration who made the SDSS project a success. Funding for creation and distribution of the SDSS Archive has been provided by the Alfred P. Sloan Foundation, Participating Institutions, NASA, NSF, DOE, the Japanese Monbukagakusho, and the Max-Planck Society. The SDSS Web site is <http://www.sdss.org>. The SDSS is managed by the Astrophysical Research Consortium for the Participating Institutions: the American Museum of Natural History, Astrophysical Institute Potsdam, University of Basel, Cambridge University, Case Western Reserve University, University of Chicago, Drexel University, Fermilab, the Institute for Advanced Study, the Japan Participation Group, Johns Hopkins University, the Joint Institute for Nuclear Astrophysics, the Kavli Institute for Particle Astrophysics and Cosmology, the Korean Scientist Group,

the Chinese Academy of Sciences (LAMOST), Los Alamos National Laboratory, the Max-Planck-Institute for Astronomy (MPIA), the Max-Planck-Institute for Astrophysics (MPA), New Mexico State University, Ohio State University, University of Pittsburgh, University of Portsmouth, Princeton University, the United States Naval Observatory, and the University of Washington

REFERENCES

- Bertin, E., & Arnouts, S. 1996, *A&A*, 117, 393
- Blanton, M. R., et al. 2003, *ApJ*, 592, 819
- Blanton, M. R., Lupton, R. H., Schlegel, D. J., Strauss, M. A., Brinkmann, J., Fukugita, M. & Loveday, J. 2005, *ApJ*, 631, 208
- Brinchmann, J., Charlot, S., White, S., Tremonti, C., Kauffmann, G., Heckman, T. & Brinkmann, J. 2004, *MNRAS*, 351, 1151
- Brown, W. R., Geller, M. J., Fabricant, D. G., & Kurtz, M. J. 2001, *AJ*, 122, 714
- Bond, N. A., Churchill, C. W., Charlton, J. C., & Vogt, S. S. 2001, *ApJ*, 562, 641
- Churchill C. W., Mellon, R. R., Charlton, J. C., Jannuzi, B. T., Kirhakos, S., Steidel, C. C., & Schneider, D. P. 2000, *ApJ*, 543, 577
- Churchill, C. W., Kacprzak, G. G., & Steidel, C. C. 2005, *IAU Colloq. 199: Probing Galaxies through Quasar Absorption Lines*, 22 (astro-ph/0505211)
- Gabasch, A. et al. 2006, *A&A*, 448, 101
- Kacprzak, G. G., Churchill, C. W., & Steidel, C. C. 2005, *IAU Colloq. 199: Probing Galaxies through Quasar Absorption Lines*, 80 (astro-ph/0505211)
- Lacy, M., Becker, R. H., Storrie-Lombardi, L. J., Gregg, M. D., Urrutia, T., & White, R. L. 2003, *AJ*, 126, 2230
- Laine, S., van der Marel, R. P., Lauer, T. R., Postman, M., O’Dea, C. P. & Owen, F. N. 2003, *AJ*, 125, 478L
- Le Brun, V., Bergeron, J., Boisse, P., & Deharveng, J. M. 1997, *A&A*, 321, 733
- McDonald, P., et al. 2006, *ApJS*, 163, 80

- Ménard, B., Nestor, D. B., Turnshek, D. A., Quider, A., Richards, G., Chelouche, D. & Rao, S. M., in prep.
- Meurer, G. et al. 2006, *ApJS*, 165, 307
- Nagashima, M., Yoshii, Y., Totani, T., & Gouda, N. 2002, *ApJ*, 578, 675
- Nakamura, O., et al. 2003, *AJ*, 125, 1682
- Nestor, D., Rao, S., Turnshek, D. & Vanden Berk, D. 2003, *ApJ*, 595, L5
- Nestor, D. B., Turnshek, D. A., & Rao, S. M. 2005, *ApJ*, 628, 637 (NTR05)
- Nestor, D. B., Turnshek, D. A., & Rao, S. M. 2006, *ApJ*, 643, 75
- Pettini, M., Rix, S. A., Steidel, C. C., Adelberger, K. L., Hunt, M. P. & Shapley, A. E. 2002, *ApJ*, 569, 742
- Prochaska, J. X., Herbert-Fort, S., & Wolfe, A. M. 2005, *ApJ*, 635, 123
- Rao, S. M., Nestor, D. B., Turnshek, D. A., Lane, W. M., Monier, E. M., & Bergeron, J. 2003, *ApJ*, 595, 94
- Rao, S. M., Turnshek, D. A., & Nestor, D. B. 2006, *ApJ*, 636, 610
- Reichard, T. A., et al. 2003, *AJ*, 25, 1711
- Savage, B. D., et al. 2000, *ApJS*, 129, 563
- Schwartz, C. M., Martin, C. L., Chandar, R., Leitherer, C., Heckman, T. M., & Oey, M. S., accepted for publication in *ApJ*, (astro-ph/0605215)
- Shapley, A. E., Steidel, C. C., Adelberger, K. L., Dickinson, M., Giavalisco, M. & Pettini, M. 2001, *ApJ*, 562, 95
- Shapley, A. E., Steidel, C. C., Pettini, M. & Adelberger, K. L. 2003, *ApJ*, 588, 65
- Steidel, C. C., Kollmeier, J. A., Shapley, A. E., Churchill, C. W., Dickinson, M., & Pettini, M. 2002, *ApJS*, 570, 526
- Tripp, T. M., & Bowen, D. V. 2005, *IAU Colloq. 199: Probing Galaxies through Quasar Absorption Lines*, 5, (astro-ph/0510312)
- Turnshek, D. A., Rao, S. M., Nestor, D. B., Belfort-Mihalyi, M., & Quider, A., 2005, *IAU Colloq. 199: Probing Galaxies through Quasar Absorption Lines*, 104 (astro-ph/0506701)

Yasuda, N., et al. 2001, AJ, 122, 1104

York, D. G., et al. 2006, MNRAS, 367, 945

Zibetti, S., Menard, B., Nestor, D., Quider, A. & Turnshek, D. submitted to ApJ (astro-ph/0609760)

Table 1.

Q0013+1414, $z_{abs} = 0.4838$, $W_0^{\lambda 2796} = 2.69 \text{ \AA}$						
$\Delta\alpha$ (arcsec)	$\Delta\delta$ (arcsec)	m_r	M_r at $z = 0.4838^a$	L/L^* at $z = 0.4838^a$	b (kpc)	projected size ^b (kpc)
1.5	−2.1	22.00	−20.49/−20.76/−20.90	0.52/0.66/0.75	15.5	17×14
5.8	4.3	19.68	−22.82/−23.08/−23.23	4.40/5.62/6.40	43.6	50×35
−9.4	16.3	21.31	−21.19/−21.45/−21.59	0.98/1.25/1.42	112.9	23×18
−7.1	27.1	21.69	−20.81/−21.08/−21.22	0.69/0.88/1.01	167.9	17×14
29.4	1.5	22.95	−19.55/−19.81/−19.95	0.22/0.28/0.31	176.7	10×9
Q0232−0811, $z_{abs} = 0.4523$, $W_0^{\lambda 2796} = 3.69 \text{ \AA}$						
$\Delta\alpha$ (arcsec)	$\Delta\delta$ (arcsec)	m_r	M_r at $z = 0.4523^a$	L/L^* at $z = 0.4523^a$	b (kpc)	projected size ^b (kpc)
0.0	0.8	22.0 ^c	−20.3/−20.5/−20.6	0.4/0.5/0.6	4.8	18×12
3.0	−8.6	21.35	−20.93/−21.17/−21.29	0.77/0.96/1.08	52.6	33×16
0.2	−16.6	22.61	−19.68/−19.91/−20.04	0.24/0.30/0.34	96.0	12×10
17.0	13.9	20.09	−22.19/−22.42/−22.55	2.47/3.06/3.44	127.0	30×28
−4.1	23.3	22.76	−19.52/−19.76/−19.88	0.21/0.26/0.29	136.9	21×9
23.2	9.6	23.96	−18.33/−18.56/−18.69	0.07/0.09/0.10	144.8	6×6
26.2	4.0	24.54	−17.74/−17.98/−18.10	0.04/0.05/0.06	152.9	4×3
17.4	−21.7	23.82	−18.46/−18.70/−18.82	0.08/0.10/0.11	160.6	9×8
19.7	21.7	22.65	−19.63/−19.87/−20.00	0.23/0.29/0.33	169.4	17×16
13.1	−26.5	21.56	−20.72/−20.96/−21.08	0.64/0.79/0.89	170.5	25×19
−26.1	−15.3	22.29	−19.99/−20.23/−20.35	0.33/0.40/0.45	174.9	15×12
−22.8	−20.6	22.79	−19.50/−19.73/−19.86	0.21/0.26/0.29	177.7	16×9
28.2	−12.6	24.20	−18.08/−18.32/−18.44	0.06/0.07/0.08	178.3	8×4
13.6	−31.5	24.55	−17.73/−17.97/−18.09	0.04/0.05/0.06	198.3	7×5
Q0240−0812, $z_{abs} = 0.5314$, $W_0^{\lambda 2796} = 2.91 \text{ \AA}$						
$\Delta\alpha$ (arcsec)	$\Delta\delta$ (arcsec)	m_r	M_r at $z = 0.5314^a$	L/L^* at $z = 0.5314^a$	b (kpc)	projected size ^b (kpc)

Table 1—Continued

2.8	0.9	20.96	−21.84/−22.15/−22.32	1.78/2.38/2.77	18.6	19×17
−8.7	8.5	22.68	−20.11/−20.42/−20.59	0.36/0.48/0.56	76.4	12×6
−4.7	11.2	21.27	−21.52/−21.84/−22.00	1.33/1.78/2.08	76.7	16×15
13.3	−2.0	22.75	−20.04/−20.36/−20.52	0.34/0.46/0.53	85.0	9×4
4.9	−12.7	21.80	−20.99/−21.30/−21.47	0.82/1.09/1.27	85.9	19×11
−3.5	−19.6	22.72	−20.07/−20.39/−20.55	0.35/0.47/0.55	125.4	10×7
8.2	26.5	21.25	−21.55/−21.86/−22.03	1.36/1.82/2.12	174.9	16×13
−28.2	−6.8	21.49	−21.30/−21.62/−21.78	1.09/1.45/1.69	182.8	17×14
27.8	8.4	23.59	−19.20/−19.51/−19.68	0.16/0.21/0.24	182.9	7×5
−8.4	29.5	22.84	−19.95/−20.27/−20.43	0.31/0.42/0.49	193.0	9×8

Q0747+3054, $z_{abs} = 0.7650$, $W_0^{\lambda 2796} = 3.63 \text{ \AA}$

$\Delta\alpha$ (arcsec)	$\Delta\delta$ (arcsec)	m_i	M_i at $z = 0.7650^a$	L/L^* at $z = 0.7650^a$	b (kpc)	projected size ^b (kpc)
−1.9	4.7	19.53	−24.20/−24.50/−24.70	11.1/14.6/17.6	37.7	47×21
4.1	3.1	21.86	−21.87/−22.17/−22.37	1.29/1.70/2.05	37.9	27×16
−5.4	−2.9	23.83	−19.90/−20.20/−20.40	0.21/0.28/0.33	45.0	8×8
−2.4	−6.0	24.33	−19.40/−19.70/−19.90	0.13/0.18/0.21	47.9	9×8
−7.8	−1.8	22.99	−20.73/−21.04/−21.24	0.45/0.60/0.72	59.1	16×11
6.8	5.3	20.67	−23.06/−23.37/−23.57	3.88/5.13/6.17	63.4	35×26
−8.4	−5.9	24.10	−19.63/−19.94/−20.14	0.16/0.22/0.26	75.8	11×6
6.5	−9.9	22.68	−21.05/−21.36/−21.56	0.61/0.81/0.97	87.7	18×13
−11.0	5.0	24.30	−19.43/−19.73/−19.93	0.14/0.18/0.22	89.1	9×5
−12.1	−1.6	24.17	−19.56/−19.86/−20.06	0.15/0.20/0.24	90.4	8×7
11.3	8.1	23.19	−20.54/−20.84/−21.04	0.38/0.50/0.61	102.9	13×11
9.5	11.3	22.73	−21.00/−21.31/−21.51	0.58/0.77/0.93	108.8	18×13
−12.9	7.6	23.98	−19.75/−20.05/−20.25	0.18/0.24/0.29	110.4	10×7
−5.9	−15.0	23.75	−19.97/−20.28/−20.48	0.23/0.30/0.36	119.0	12×6
−16.1	7.9	24.08	−19.65/−19.95/−20.15	0.17/0.22/0.27	132.5	10×8
−13.4	12.2	23.65	−20.07/−20.38/−20.58	0.25/0.33/0.39	134.0	9×8
−15.9	14.4	24.01	−19.72/−20.02/−20.22	0.18/0.24/0.28	158.2	9×8
−12.5	18.3	23.76	−19.97/−20.28/−20.48	0.23/0.30/0.36	163.7	9×8
−22.9	−3.2	23.91	−19.82/−20.13/−20.33	0.20/0.26/0.31	171.0	8×6

Table 1—Continued

13.3	−20.0	24.80	−18.93/−19.23/−19.43	0.09/0.11/0.14	177.7	9×4
17.6	17.3	23.99	−19.73/−20.04/−20.24	0.18/0.24/0.29	182.4	9×8
16.0	−19.3	23.86	−19.87/−20.17/−20.37	0.20/0.27/0.33	185.4	9×8
−23.1	−9.9	22.72	−21.01/−21.31/−21.51	0.59/0.78/0.93	185.8	17×13
16.9	19.3	22.79	−20.94/−21.24/−21.44	0.55/0.73/0.87	189.4	12×12
8.7	24.3	24.84	−18.89/−19.20/−19.40	0.08/0.11/0.13	190.9	7×6
−23.5	−11.2	23.26	−20.47/−20.78/−20.98	0.36/0.47/0.57	192.0	13×11

Q0747+3354, $z_{abs} = 0.6202$, $W_0^{\lambda 2796} = 4.69 \text{ \AA}$

$\Delta\alpha$ (arcsec)	$\Delta\delta$ (arcsec)	M_i at $z = 0.6202^a$	L/L^* at $z = 0.6202^a$	b (kpc)	projected size ^b (kpc)
1.7	0.9	21.11	−21.95/−22.16/−22.32	1.39/1.70/1.96	32×22
0.2	5.1	23.14	−19.92/−20.14/−20.29	0.22/0.26/0.30	11×9
11.4	−10.3	22.20	−20.87/−21.08/−21.24	0.51/0.62/0.72	16×15
−18.0	−5.0	22.55	−20.52/−20.73/−20.89	0.37/0.45/0.52	18×14
−11.7	−14.7	23.72	−19.35/−19.56/−19.72	0.13/0.15/0.18	9×4
−19.0	−6.5	21.86	−21.21/−21.42/−21.58	0.70/0.86/0.99	18×17
−2.9	25.5	21.69	−21.38/−21.59/−21.75	0.82/1.00/1.15	18×17

Q0800+2150, $z_{abs} = 0.5716$, $W_0^{\lambda 2796} = 3.65 \text{ \AA}$

$\Delta\alpha$ (arcsec)	$\Delta\delta$ (arcsec)	M_r at $z = 0.5716^a$	L/L^* at $z = 0.5716^a$	b (kpc)	projected size ^b (kpc)
2.6	1.2	22.22	−20.84/−21.20/−21.39	0.71/0.99/1.19	21×15
2.6	−1.3	24.63	−18.42/−18.79/−18.98	0.08/0.11/0.13	9×8
−0.8	−6.7	23.98	−19.08/−19.44/−19.63	0.14/0.20/0.23	11×8
6.2	5.9	24.73	−18.33/−18.69/−18.88	0.07/0.10/0.12	12×4
−8.3	2.5	23.66	−19.39/−19.76/−19.95	0.19/0.26/0.31	12×11
8.5	3.1	24.38	−18.67/−19.04/−19.23	0.10/0.14/0.16	10×9
7.4	13.7	23.28	−19.78/−20.14/−20.33	0.27/0.37/0.45	16×14
−7.3	14.1	22.28	−20.78/−21.14/−21.33	0.67/0.94/1.12	20×15
11.8	−10.8	24.55	−18.51/−18.87/−19.06	0.08/0.12/0.14	8×7
6.3	−15.7	24.96	−18.10/−18.46/−18.65	0.06/0.08/0.10	7×5

Table 1—Continued

−17.7	4.7	21.96	−21.10/−21.46/−21.65	0.90/1.26/1.50	119.6	12 × 12
−2.8	−23.5	24.89	−18.16/−18.53/−18.72	0.06/0.08/0.10	154.4	8 × 6
−9.6	−22.8	23.15	−19.90/−20.27/−20.46	0.30/0.42/0.50	161.7	15 × 13
−23.3	−9.7	25.00	−18.06/−18.42/−18.61	0.05/0.08/0.09	165.2	7 × 5
9.3	−23.5	24.59	−18.46/−18.83/−19.02	0.08/0.11/0.13	165.2	9 × 6
−9.2	23.6	21.67	−21.38/−21.75/−21.94	1.17/1.64/1.96	165.6	20 × 14
9.8	25.1	24.38	−18.67/−19.03/−19.23	0.10/0.13/0.16	175.8	9 × 9
−6.5	26.6	24.85	−18.20/−18.57/−18.76	0.06/0.09/0.10	179.0	6 × 6
14.7	−23.8	24.68	−18.38/−18.74/−18.93	0.07/0.10/0.12	182.7	9 × 7
−18.2	21.2	24.22	−18.83/−19.20/−19.39	0.11/0.16/0.19	182.7	10 × 7
25.9	−12.0	19.81	−23.25/−23.61/−23.80	6.52/9.12/10.9	186.7	60 × 38
11.6	−26.8	23.85	−19.21/−19.57/−19.76	0.16/0.22/0.26	190.9	14 × 8
−21.8	−19.5	23.24	−19.81/−20.18/−20.37	0.28/0.39/0.46	191.3	12 × 11
−0.2	−29.4	21.59	−21.47/−21.83/−22.02	1.27/1.77/2.11	192.3	20 × 15
13.5	−26.6	23.46	−19.60/−19.96/−20.15	0.23/0.32/0.38	194.9	13 × 11

Q0836+5132, $z_{abs} = 0.5666$, $W_0^{\lambda 2796} = 3.48 \text{ \AA}$

$\Delta\alpha$ (arcsec)	$\Delta\delta$ (arcsec)	m_r	M_r at $z = 0.5666^a$	L/L^* at $z = 0.5666^a$	b (kpc)	projected size ^b (kpc)
−0.6	−1.4	23.02	−20.01/−20.36/−20.55	0.33/0.46/0.55	10.1	22 × 18
9.2	−1.4	24.74	−18.29/−18.65/−18.83	0.07/0.09/0.11	60.4	6 × 4
3.3	−11.6	23.18	−19.84/−20.20/−20.38	0.28/0.39/0.47	78.6	18 × 16
4.1	17.0	21.68	−21.34/−21.70/−21.89	1.13/1.57/1.87	113.9	35 × 26
5.8	19.6	20.71	−22.32/−22.68/−22.86	2.78/3.86/4.59	133.1	45 × 38
−19.7	−10.2	23.51	−19.51/−19.87/−20.06	0.21/0.29/0.35	144.0	11 × 8
−16.1	−20.9	17.09 ^d	172.0	...
16.4	21.8	20.84	−22.18/−22.54/−22.73	2.45/3.41/4.05	177.9	52 × 31

Q0902+3722, $z_{abs} = 0.6697$, $W_0^{\lambda 2796} = 3.97 \text{ \AA}$

$\Delta\alpha$ (arcsec)	$\Delta\delta$ (arcsec)	m_i	M_i at $z = 0.6697^a$	L/L^* at $z = 0.6697^a$	b (kpc)	projected size ^b (kpc)
2.2	−1.4	21.42	−21.89/−22.13/−22.30	1.32/1.64/1.92	18.4	20 × 18

Table 1—Continued

−4.6	2.3	22.38	−20.92/−21.17/−21.34	0.54/0.68/0.79	35.8	16 × 14
4.8	−2.1	21.70	−21.61/−21.85/−22.02	1.02/1.27/1.49	36.8	29 × 15
−5.4	−12.1	22.60	−20.71/−20.95/−21.12	0.44/0.55/0.65	92.8	11 × 11
−10.7	9.4	23.93	−19.37/−19.61/−19.78	0.13/0.16/0.19	99.8	9 × 5
14.5	10.0	22.99	−20.31/−20.55/−20.73	0.31/0.39/0.45	123.4	10 × 6
−0.0	−18.7	23.13	−20.18/−20.42/−20.59	0.27/0.34/0.40	131.2	9 × 8
−7.8	17.8	21.69	−21.61/−21.85/−22.02	1.02/1.27/1.49	136.5	24 × 16
−8.6	−19.8	23.94	−19.37/−19.61/−19.78	0.13/0.16/0.19	151.6	8 × 5
4.6	21.5	23.38	−19.92/−20.16/−20.33	0.22/0.27/0.31	154.1	10 × 9
6.9	23.7	20.30	−23.00/−23.24/−23.41	3.67/4.58/5.36	172.8	24 × 16
−24.8	4.6	20.69	−22.62/−22.86/−23.03	2.58/3.22/3.77	177.0	42 × 17
−24.7	8.9	21.07	−22.24/−22.48/−22.65	1.82/2.27/2.65	184.4	34 × 15
−11.2	−23.9	23.45	−19.85/−20.09/−20.26	0.20/0.25/0.29	185.4	9 × 8
−3.3	26.9	23.21	−20.09/−20.33/−20.51	0.25/0.31/0.37	190.3	10 × 9

Q1000+4438, $z_{abs} = 0.7192$, $W_0^{\lambda 2796} = 5.33 \text{ \AA}$

$\Delta\alpha$ (arcsec)	$\Delta\delta$ (arcsec)	m_i	M_i at $z = 0.7192^a$	L/L^* at $z = 0.7192^a$	b (kpc)	projected size ^b (kpc)
0.8	0.8	21.5 ^c	−22.0/−22.3/−22.5	1.5/1.9/2.3	8.4	28 × 22
4.1	4.6	23.94	−19.60/−19.87/−20.05	0.16/0.20/0.24	44.4	11 × 10
5.7	13.7	22.77	−20.76/−21.04/−21.22	0.47/0.60/0.71	107.2	18 × 11
−17.2	−5.8	20.91	−22.62/−22.89/−23.08	2.58/3.32/3.94	131.1	33 × 32
1.8	19.8	22.73	−20.80/−21.07/−21.26	0.48/0.62/0.74	144.0	17 × 9
19.4	7.3	23.06	−20.48/−20.75/−20.94	0.36/0.46/0.55	149.7	18 × 16
4.8	22.4	21.31	−22.22/−22.49/−22.68	1.79/2.30/2.72	165.5	31 × 22
−18.7	−18.1	22.57	−20.97/−21.24/−21.42	0.56/0.72/0.86	188.1	19 × 16
−17.2	−19.6	21.22	−22.32/−22.59/−22.77	1.95/2.51/2.98	188.7	22 × 20
13.0	−24.3	23.85	−19.69/−19.96/−20.14	0.17/0.22/0.26	199.4	8 × 6
−27.5	−2.6	23.80	−19.73/−20.00/−20.19	0.18/0.23/0.27	199.7	11 × 9

Q1011+4451, $z_{abs} = 0.8360$, $W_0^{\lambda 2796} = 4.94 \text{ \AA}$

$\Delta\alpha$ (arcsec)	$\Delta\delta$ (arcsec)	M_i at m_i $z = 0.8360^a$	L/L^* at $z = 0.8360^a$	b (kpc)	projected size ^b (kpc)
----------------------------	----------------------------	-------------------------------------	------------------------------	--------------	--------------------------------------

Table 1—Continued

−0.1	2.6	24.45	−19.59/−19.95/−20.18	0.16/0.22/0.27	20.0	8 × 6
1.5	−3.9	20.63	−23.41/−23.77/−24.00	5.34/7.44/9.18	32.1	27 × 22
−5.8	1.0	21.10	−22.95/−23.31/−23.53	3.49/4.86/5.99	44.8	29 × 23
−4.3	4.3	24.10	−19.94/−20.30/−20.53	0.22/0.31/0.38	46.3	13 × 5
7.9	5.5	23.79	−20.25/−20.61/−20.84	0.29/0.41/0.50	73.6	11 × 9
8.7	−5.7	23.35	−20.69/−21.05/−21.28	0.44/0.61/0.75	79.5	12 × 11
−8.7	8.1	24.58	−19.46/−19.82/−20.05	0.14/0.20/0.24	90.7	9 × 6
9.2	−10.0	23.79	−20.25/−20.61/−20.84	0.29/0.41/0.50	103.3	15 × 7
12.9	11.0	24.74	−19.30/−19.66/−19.89	0.12/0.17/0.21	128.9	10 × 5
9.6	−16.9	22.87	−21.17/−21.53/−21.76	0.68/0.95/1.17	148.0	15 × 11
−16.7	11.2	21.78	−22.27/−22.63/−22.85	1.86/2.60/3.20	153.1	20 × 17
19.9	3.6	23.82	−20.22/−20.58/−20.81	0.28/0.39/0.49	153.9	16 × 8
−10.2	−18.9	24.10	−19.94/−20.30/−20.53	0.22/0.31/0.38	163.6	12 × 9
20.2	7.6	22.66	−21.38/−21.74/−21.97	0.82/1.15/1.41	164.2	18 × 16
−8.0	20.4	24.89	−19.15/−19.51/−19.74	0.11/0.15/0.18	166.8	8 × 5
−19.9	−9.3	21.62	−22.42/−22.78/−23.01	2.15/2.99/3.69	167.2	16 × 15
20.4	10.1	23.45	−20.59/−20.95/−21.18	0.40/0.56/0.69	173.6	11 × 10
−24.4	−0.3	22.54	−21.51/−21.87/−22.09	0.92/1.29/1.59	185.8	14 × 12
−24.4	−8.4	16.78	−27.26/−27.62/−27.85	186/259/320	196.8	192 × 35

Q1038+4727, $z_{abs} = 0.5292$, $W_0^{\lambda 2796} = 3.14 \text{ \AA}$

$\Delta\alpha$ (arcsec)	$\Delta\delta$ (arcsec)	m_r	M_r at $z = 0.5292^a$	L/L^* at $z = 0.5292^a$	b (kpc)	projected size ^b (kpc)
−1.9	1.3	21.12	−21.66/−21.97/−22.13	1.51/2.01/2.34	14.8	28 × 16
−4.6	3.0	23.01	−19.78/−20.09/−20.25	0.27/0.36/0.41	34.9	12 × 7
−15.9	3.1	21.33	−21.46/−21.77/−21.93	1.25/1.67/1.95	102.1	22 × 20
7.1	21.7	22.64	−20.14/−20.45/−20.62	0.37/0.50/0.58	143.8	15 × 12
−22.9	8.6	22.75	−20.03/−20.35/−20.51	0.34/0.45/0.52	153.8	12 × 11
−24.4	4.7	22.78	−20.00/−20.31/−20.47	0.33/0.44/0.51	156.5	11 × 10
21.6	13.3	23.28	−19.50/−19.82/−19.98	0.21/0.28/0.32	159.6	10 × 9
21.8	−19.2	23.43	−19.36/−19.67/−19.83	0.18/0.24/0.28	182.8	14 × 7
27.5	−13.9	23.57	−19.21/−19.53/−19.69	0.16/0.21/0.25	193.7	10 × 6

Table 1—Continued

1.5	30.8	22.38	−20.40/−20.71/−20.87	0.47/0.63/0.73	194.0	13×12
Q1356+6119, $z_{abs} = 0.7850$, $W_0^{\lambda 2796} = 5.97 \text{ \AA}$						
$\Delta\alpha$ (arcsec)	$\Delta\delta$ (arcsec)	m_i	M_i at $z = 0.7850^a$	L/L^* at $z = 0.7850^a$	b (kpc)	projected size ^b (kpc)
−1.0	0.5	21.7 ^c	−22.1/−22.5/−22.7	1.7/2.2/2.7	8.6	22×17
−0.3	6.7	22.02	−21.79/−22.11/−22.32	1.21/1.62/1.96	50.4	21×17
7.3	6.5	22.81	−21.01/−21.33/−21.53	0.59/0.79/0.95	72.7	18×14
−1.5	10.6	23.15	−20.66/−20.98/−21.19	0.43/0.57/0.69	79.5	15×12
13.3	−7.8	22.05 ^e	−21.77/−22.09/−22.29	1.18/1.58/1.91	114.8	16×14
14.3	−9.0	24.05	−19.76/−20.08/−20.29	0.19/0.25/0.30	126.2	12×6
−7.6	17.7	21.95	−21.87/−22.19/−22.39	1.29/1.73/2.10	143.7	17×15
18.8	6.6	23.90	−19.91/−20.23/−20.44	0.21/0.29/0.35	148.8	8×7
−1.8	21.4	19.94	−23.87/−24.19/−24.40	8.19/11.0/13.3	159.8	37×35
19.7	−8.7	22.41	−21.41/−21.73/−21.93	0.85/1.13/1.37	161.0	19×15
−21.6	−5.2	20.32	−23.49/−23.81/−24.02	5.78/7.73/9.36	165.9	49×25
20.9	−8.2	23.36	−20.46/−20.78/−20.98	0.35/0.47/0.57	167.5	14×10
−15.6	−19.8	20.74	−23.08/−23.40/−23.60	3.94/5.28/6.39	188.0	28×23
−24.8	5.3	19.64	−24.18/−24.49/−24.70	10.8/14.5/17.6	188.9	39×29
−17.8	19.0	18.81	−25.01/−25.33/−25.53	23.3/31.2/37.8	194.0	75×48
−7.4	25.0	23.14	−20.68/−20.99/−21.20	0.43/0.58/0.70	194.6	14×12
4.9	26.0	22.98	−20.84/−21.15/−21.36	0.50/0.67/0.81	197.1	14×10
−25.4	7.5	22.29	−21.52/−21.84/−22.05	0.94/1.26/1.52	197.5	20×16
−19.7	−18.0	22.46	−21.36/−21.68/−21.88	0.81/1.08/1.31	199.1	25×15
Q1417+0115, $z_{abs} = 0.6687$, $W_0^{\lambda 2796} = 5.6 \text{ \AA}$						
$\Delta\alpha$ (arcsec)	$\Delta\delta$ (arcsec)	m_i	M_i at $z = 0.6687^a$	L/L^* at $z = 0.6687^a$	b (kpc)	projected size ^b (kpc)
−2.5	−3.3	21.86	−21.44/−21.68/−21.85	0.87/1.09/1.28	29.0	19×12
−6.4	−5.0	23.26	−20.04/−20.28/−20.45	0.24/0.30/0.35	57.1	7×4
6.7	5.3	20.33	−22.97/−23.21/−23.38	3.57/4.46/5.21	60.0	27×25
11.0	−2.4	23.01	−20.29/−20.54/−20.71	0.30/0.38/0.44	79.2	12×7

Table 1—Continued

7.0	−10.1	19.32	−23.98/−24.22/−24.39	9.02/11.3/13.2	86.3	42×38
18.4	−1.2	21.15	−22.15/−22.39/−22.56	1.68/2.09/2.45	129.2	26×20
−11.6	14.8	22.34	−20.96/−21.20/−21.37	0.56/0.70/0.81	132.1	15×8
−23.0	1.9	21.27	−22.03/−22.27/−22.44	1.50/1.87/2.18	162.1	26×19
−20.5	−12.1	20.78	−22.52/−22.76/−22.93	2.35/2.93/3.43	166.5	30×23
−9.7	−23.2	21.90	−21.40/−21.64/−21.81	0.84/1.05/1.23	176.5	18×16
−19.3	−20.3	22.36	−20.94/−21.18/−21.35	0.55/0.68/0.80	196.4	13×12

Q1427+5325, $z_{abs} = 0.5537$, $W_0^{\lambda 2796} = 4.35 \text{ \AA}$

$\Delta\alpha$ (arcsec)	$\Delta\delta$ (arcsec)	m_r	M_r at $z = 0.5537^a$	L/L^* at $z = 0.5537^a$	b (kpc)	projected size ^b (kpc)
1.7	0.7	21.3 ^c	−21.7/−22.0/−22.2	1.6/2.1/2.5	11.7	31 × 25
0.4	−2.4	22.3 ^c	−20.6/−20.9/−21.1	0.6/0.8/0.9	15.4	25 × 19
2.7	2.3	22.1 ^c	−20.9/−21.2/−21.4	0.7/1.0/1.2	23.1	21 × 20
−5.3	1.4	23.78 ^e	−19.16/−19.50/−19.68	0.15/0.21/0.24	35.5	9 × 7
6.4	−1.1	21.82	−21.12/−21.46/−21.64	0.92/1.26/1.49	41.8	18 × 18
−12.1	4.5	23.31	−19.63/−19.97/−20.15	0.23/0.32/0.38	83.2	13 × 8
14.8	−0.8	21.48	−21.46/−21.80/−21.98	1.26/1.72/2.03	95.1	34 × 20
−15.7	−14.5	22.98	−19.96/−20.30/−20.48	0.32/0.43/0.51	137.3	15 × 12
9.0	20.0	24.21	−18.73/−19.07/−19.25	0.10/0.14/0.16	141.3	11 × 4
−25.0	−12.6	23.46	−19.48/−19.82/−20.00	0.20/0.28/0.33	180.0	10 × 8
−20.9	−21.7	21.12	−21.82/−22.16/−22.34	1.75/2.39/2.82	193.5	36 × 30

Q1520+6105, $z_{abs} = 0.4235$, $W_0^{\lambda 2796} = 4.24 \text{ \AA}$

$\Delta\alpha$ (arcsec)	$\Delta\delta$ (arcsec)	m_r	M_r at $z = 0.4235^a$	L/L^* at $z = 0.4235^a$	b (kpc)	projected size ^b (kpc)
−2.7	2.3	19.72	−22.36/−22.57/−22.69	2.89/3.51/3.90	19.6	31×19
13.1	−6.6	22.90	−19.18/−19.39/−19.51	0.15/0.19/0.21	81.4	9×8
15.8	13.1	21.00	−21.08/−21.30/−21.41	0.89/1.08/1.20	113.9	14×12
12.1	−17.7	22.83	−19.26/−19.47/−19.59	0.17/0.20/0.22	119.4	8×7
2.0	−23.7	22.56	−19.52/−19.73/−19.85	0.21/0.26/0.28	132.3	12×10
−9.0	−22.7	20.25	−21.84/−22.05/−22.17	1.78/2.17/2.41	135.9	25×24

Table 1—Continued

20.1	−15.7	19.91	−22.18/−22.39/−22.50	2.43/2.96/3.29	142.0	23×20
11.8	−24.6	22.84	−19.24/−19.45/−19.57	0.16/0.20/0.22	151.8	13×8
−23.0	22.4	22.76	−19.33/−19.54/−19.66	0.18/0.21/0.24	178.4	11×9
20.9	25.8	20.49	−21.59/−21.80/−21.92	1.42/1.72/1.92	184.5	25×20
−21.5	−25.4	22.71	−19.38/−19.59/−19.70	0.18/0.22/0.25	185.0	12×8

^aUsing Sc/Sa/E k -corrections.

^bApproximate optical extent if at $z = z_{abs}$.

^cApproximate value due to blending with quasar PSF residuals.

^dSDSS spectroscopic redshift of $z = 0.113$.

^eObject is only marginally resolved and may be a star.

Table 2. Tentative Environment Descriptions

Sightline	$W_0^{\lambda 2796}$	z_{abs}	Galaxy Overlaps Sightline?	Evidence for Pair?	$L \geq 4L^*$ and $b < 90$ kpc? ^a	Category
0013+1414	2.69	0.484	no	yes	yes	norm./inter.
0240–0812	2.91	0.531	no	no	no	normal
1038+4727	3.14	0.529	no	close	no	normal
0836+5132	3.48	0.567	close	no	no	normal
0747+3054	3.63	0.765	no	yes	yes	bright/inter.
0800+2150	3.65	0.572	no	yes	no	norm./inter.
0232–0811	3.69	0.452	yes	no	no	overlap
0902+3722	3.97	0.670	no	yes	no	norm./inter.
1520+6105	4.24	0.423	close	no	no	normal
1427+5325	4.35	0.554	yes	yes	no	overlap/inter.
0747+3354	4.69	0.620	yes	close	no	overlap
1011+4451	4.94	0.836	no	close	yes	bright
1000+4438	5.33	0.719	yes	no	no	overlap
1417+0115	5.6	0.669	no	no	yes	bright
1356+6119	5.97	0.785	yes	no	no	overlap

^aFor $z_{gal} = z_{abs}$

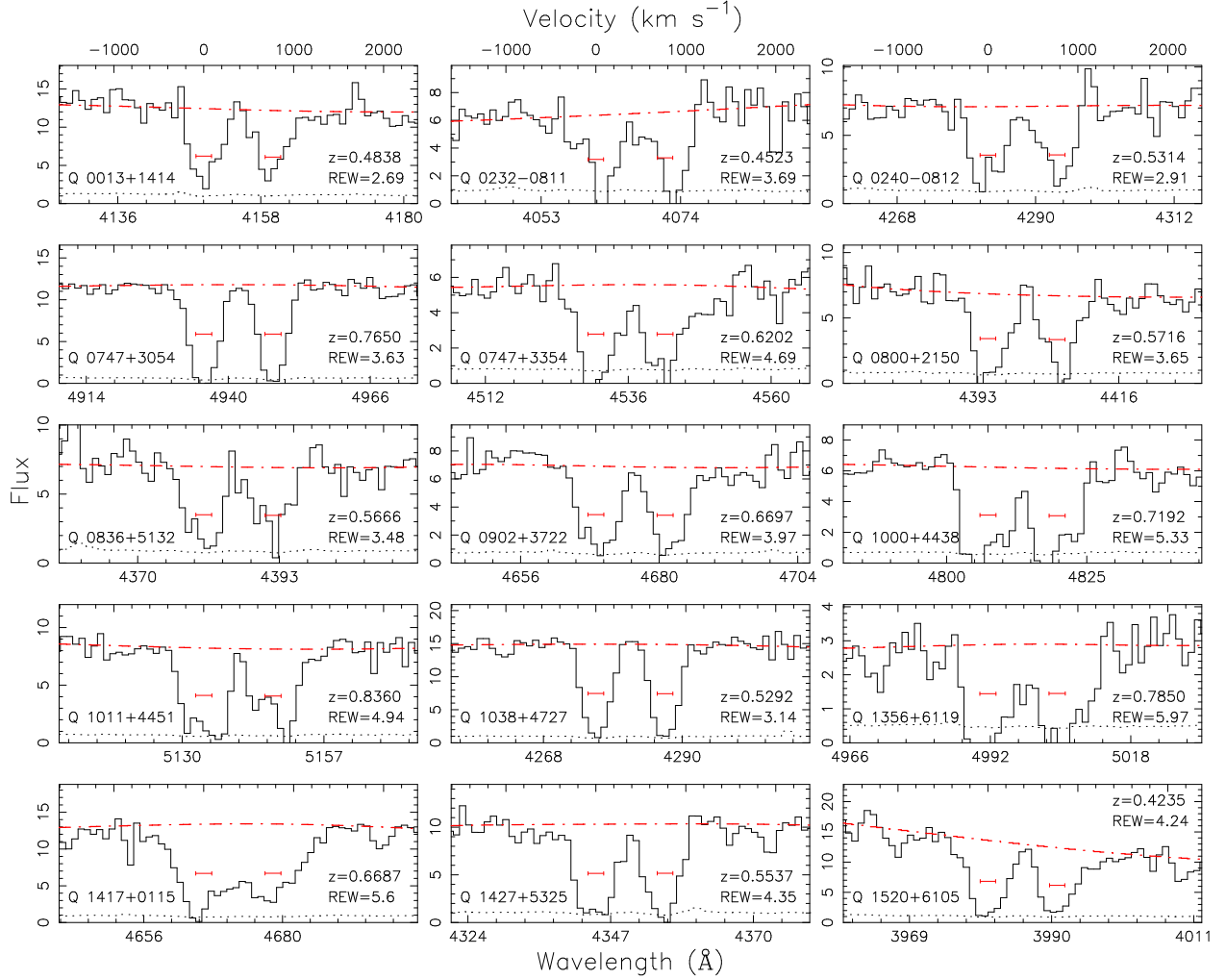


Fig. 1.— Absorption region of the SDSS spectra containing ultra-strong Mg II absorption systems. Horizontal bars indicate the resolution FWHM. The top x-axes show rest-frame velocity relative to λ2796.

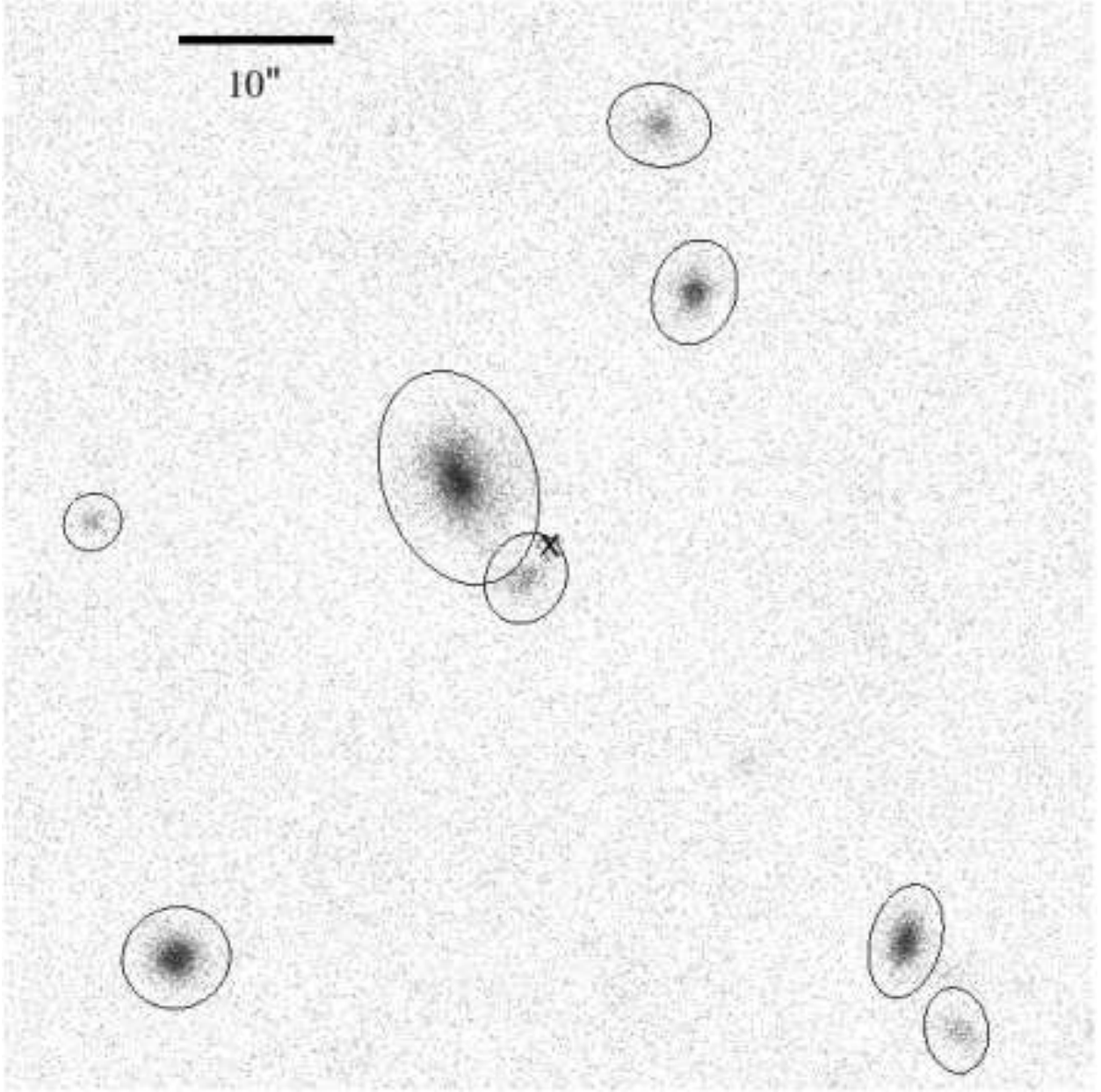


Fig. 2.— WIYN r' image of the Q0013+1414 field. The absorption has $z_{abs} = 0.4838$ and $W_0^{\lambda 2796} = 2.69 \text{ \AA}$. At the absorption redshift, $10''$ corresponds to 60.0 kpc. In the following figures, ellipses represent photometric integration limits (twice the isophotal limit, see § 3) and unless otherwise noted the quasar PSF has been subtracted and it's location marked with the symbol “x”.

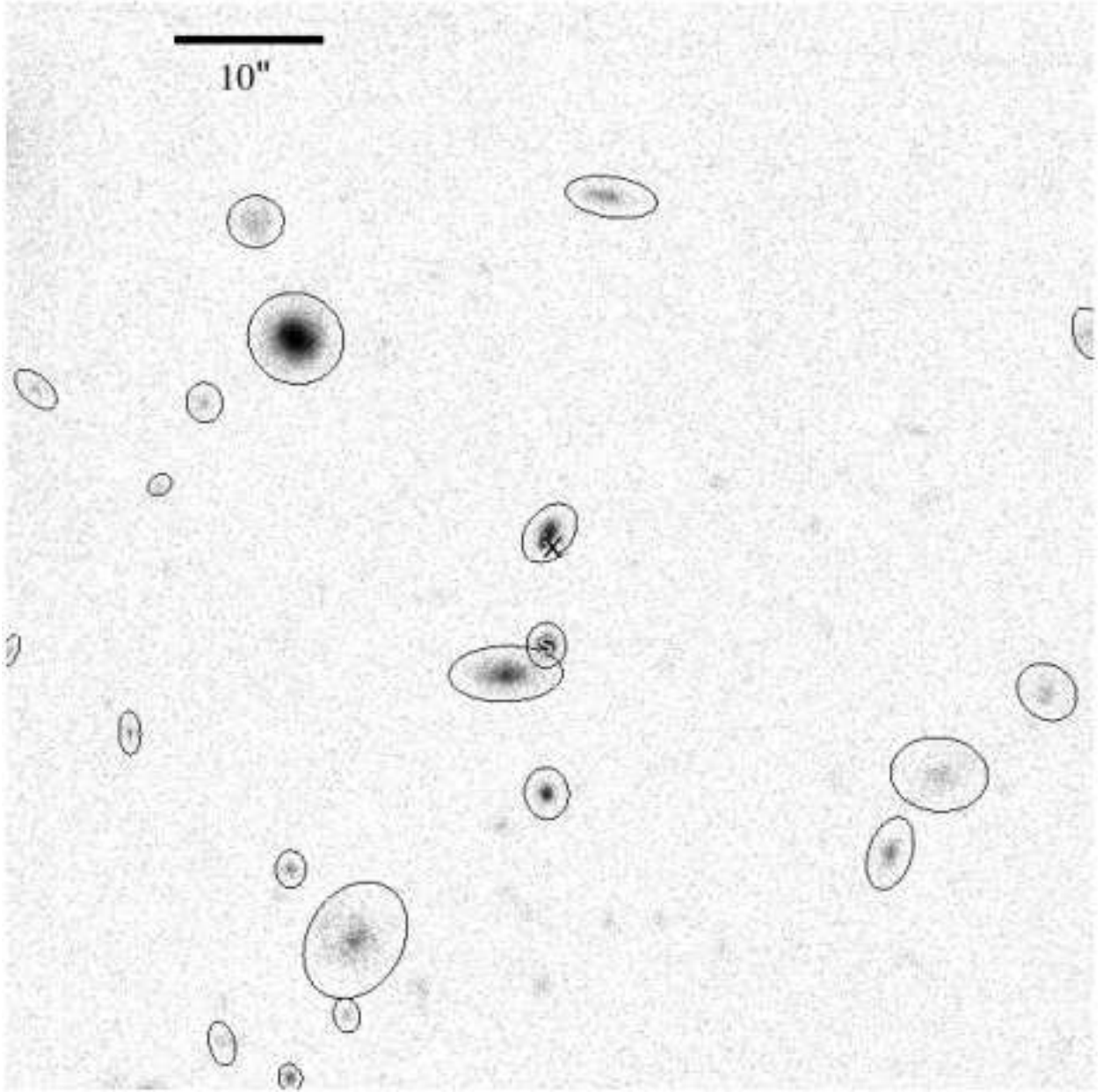


Fig. 3.— WIYN r' image of the Q0232-0811 field. The absorption has $z_{abs} = 0.4523$ and $W_0^{\lambda 2796} = 3.69 \text{ \AA}$. At the absorption redshift, $10''$ corresponds to 57.8 kpc.

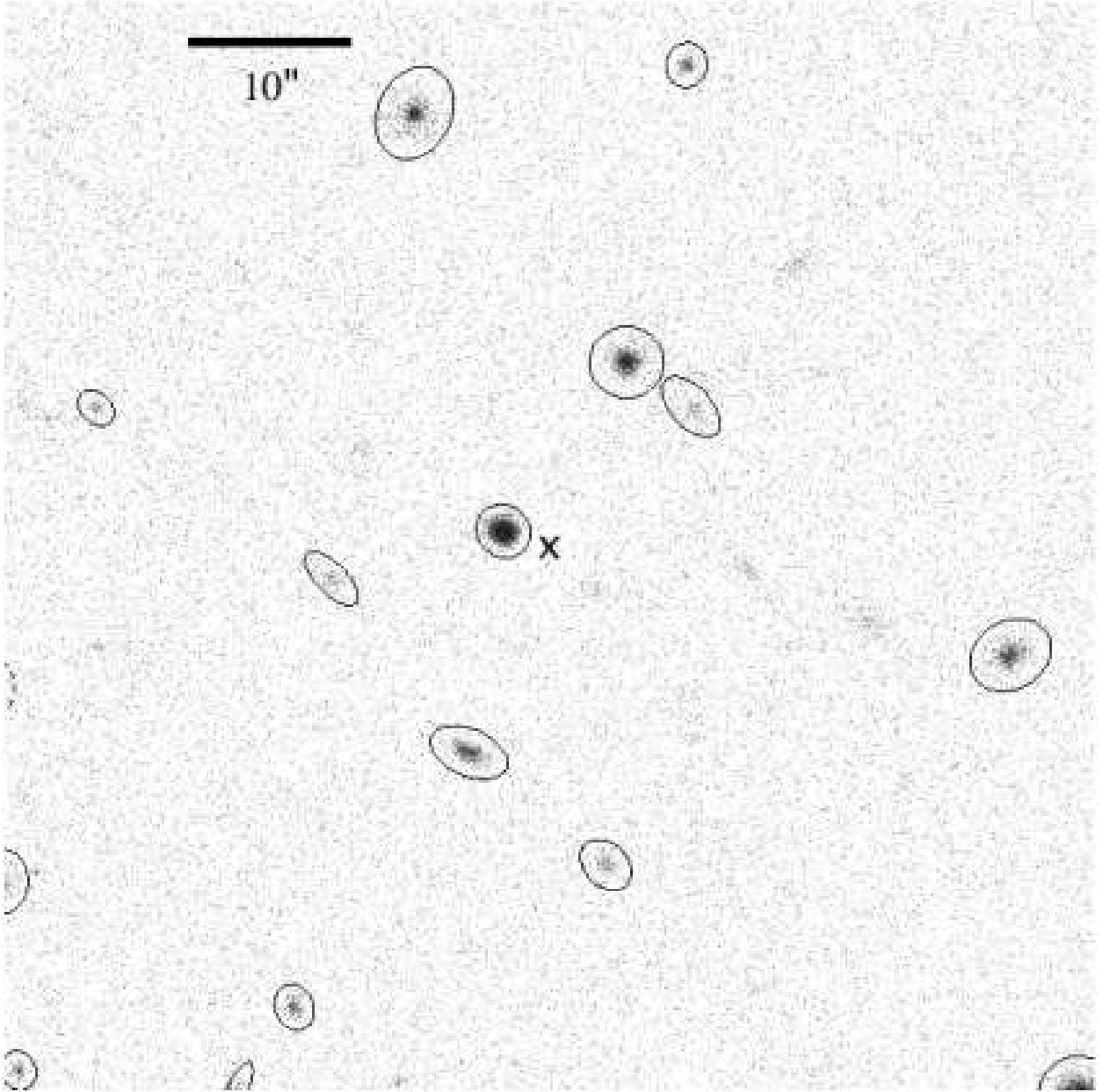


Fig. 4.— WIYN r' image of the Q0240-0812 field. The absorption has $z_{abs} = 0.5313$ and $W_0^{\lambda 2796} = 2.91 \text{ \AA}$. At the absorption redshift, $10''$ corresponds to 63.0 kpc.

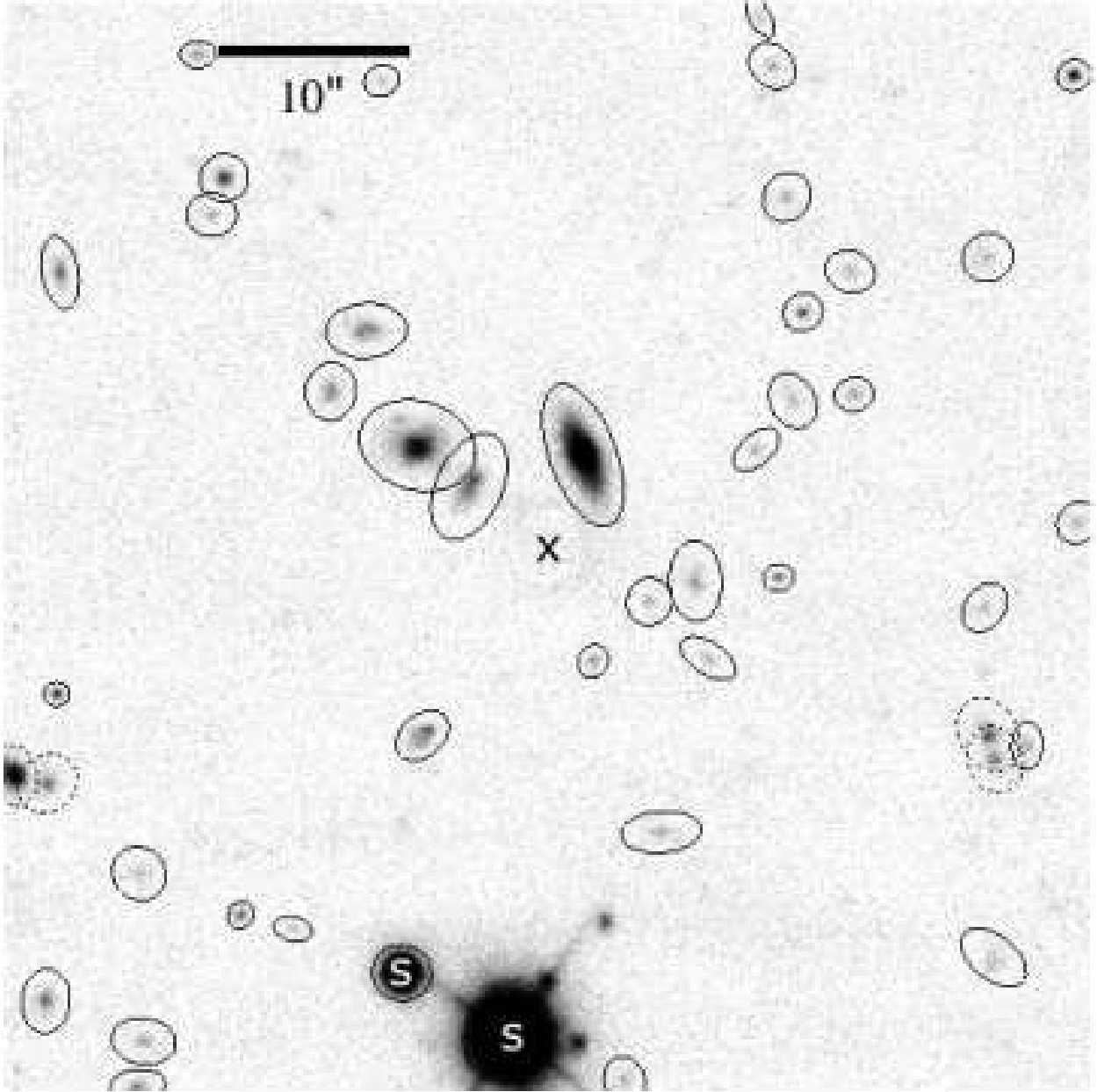


Fig. 5.— WIYN i' image of the Q0747+3054 field. The absorption has $z_{abs} = 0.7650$ and $W_0^{\lambda 2796} = 3.63 \text{ \AA}$. At the absorption redshift, $10''$ corresponds to 73.9 kpc.

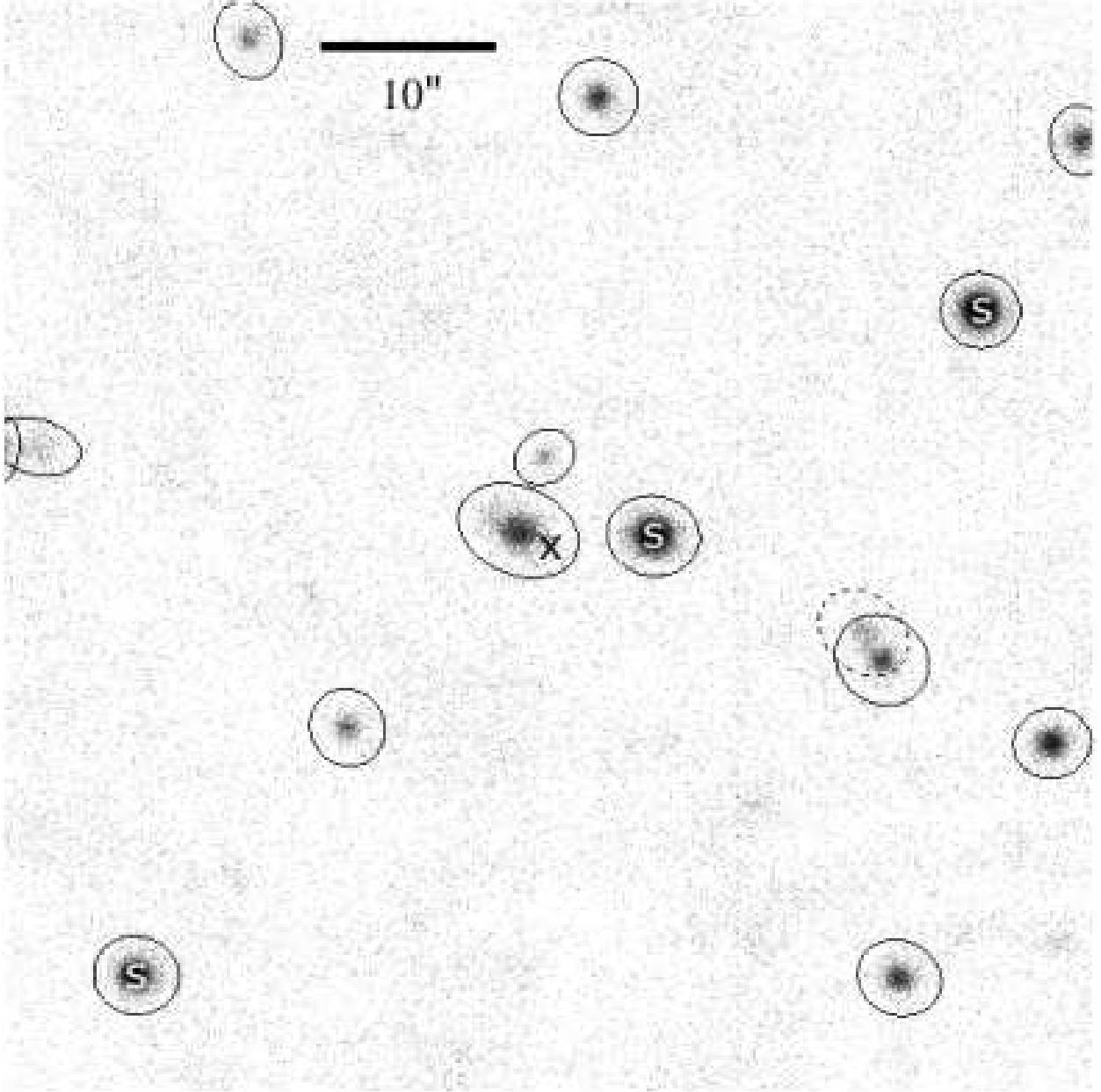


Fig. 6.— WIYN i' image of the Q0747+3354 field. The absorption has $z_{abs} = 0.6202$ and $W_0^{\lambda 2796} = 4.69 \text{ \AA}$. At the absorption redshift, $10''$ corresponds to 67.9 kpc.

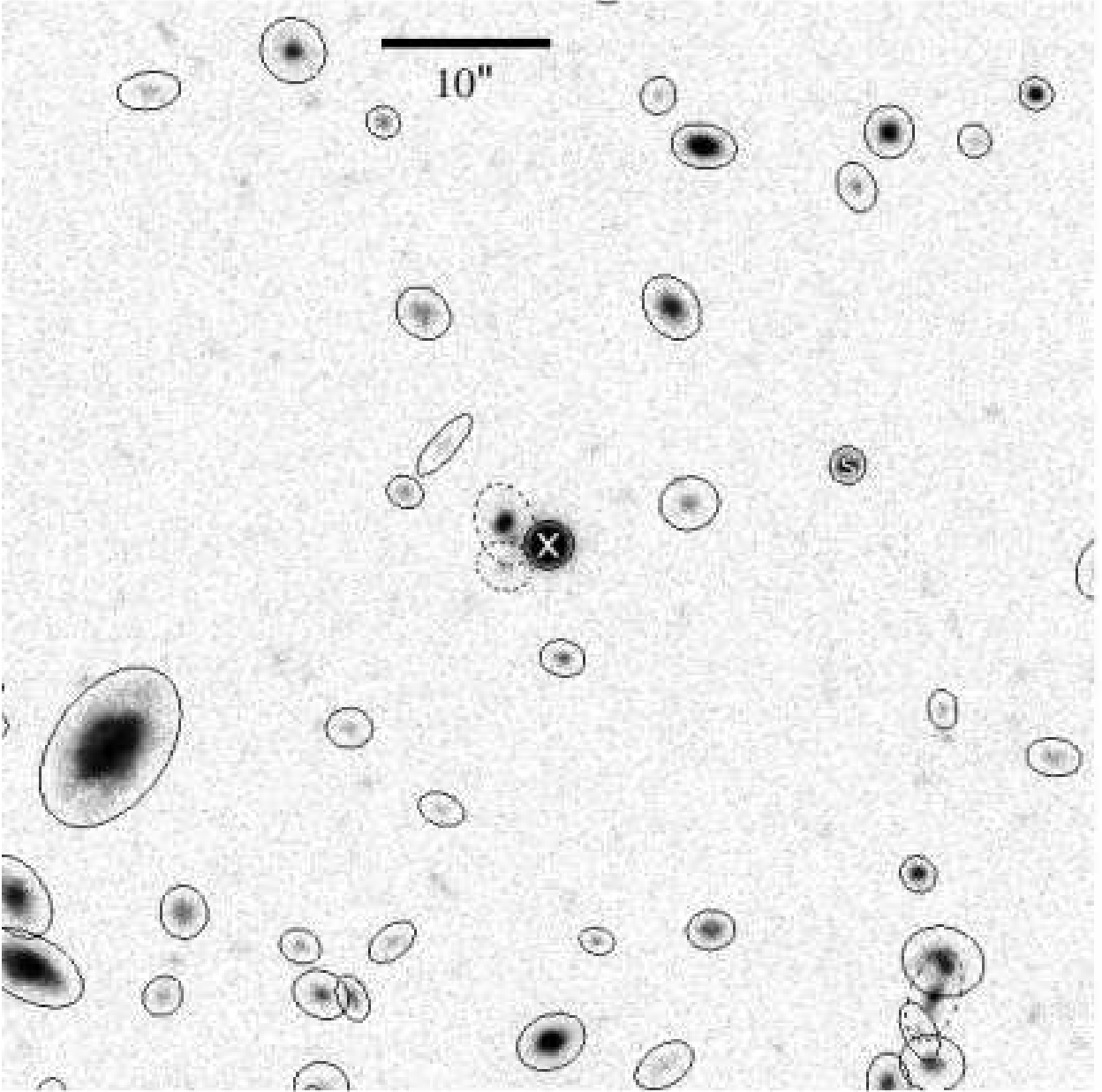


Fig. 7.— WIYN r' image of the Q0800+2150 field. The absorption has $z_{abs} = 0.5716$ and $W_0^{\lambda 2796} = 3.65 \text{ \AA}$. At the absorption redshift, $10''$ corresponds to 65.3 kpc. The quasar PSF has not been subtracted in this image.

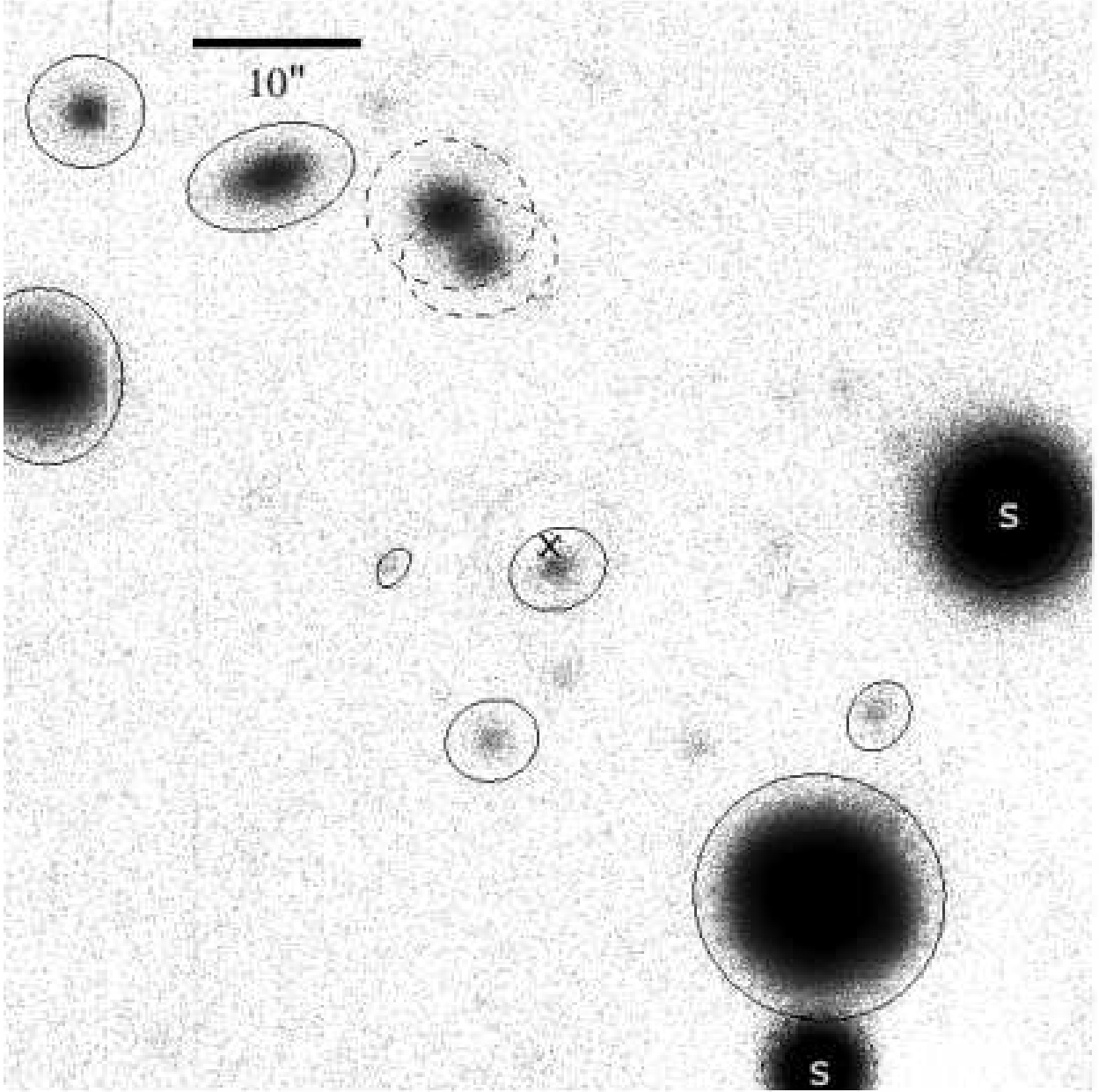


Fig. 8.— WIYN r' image of the Q0836+5132 field. The absorption has $z_{abs} = 0.5666$ and $W_0^{\lambda 2796} = 3.48 \text{ \AA}$. At the absorption redshift, $10''$ corresponds to 65.1 kpc.

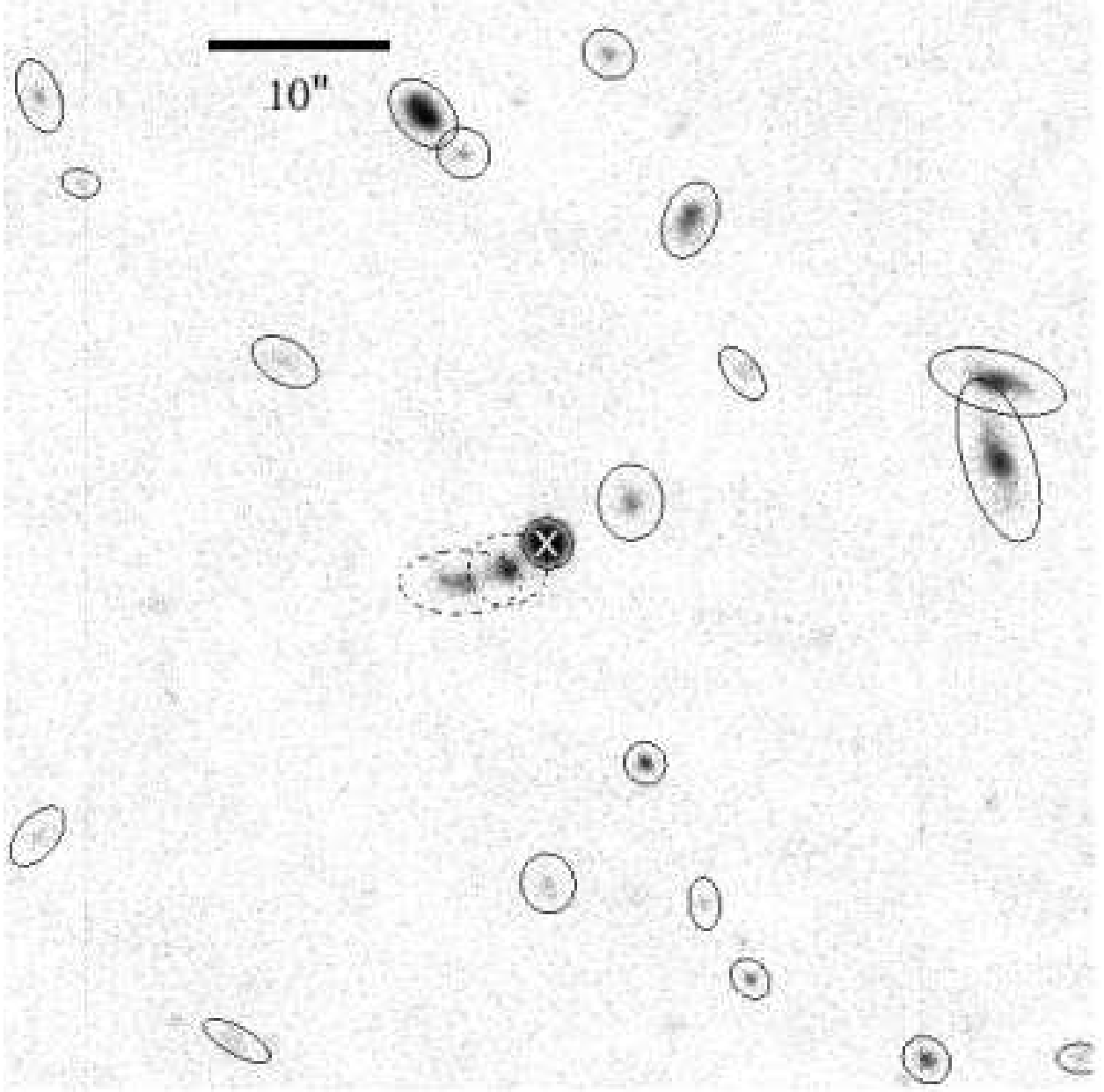


Fig. 9.— WIYN i' image of the Q0902+3722 field. The absorption has $z_{abs} = 0.6697$ and $W_0^{\lambda 2796} = 3.97 \text{ \AA}$. At the absorption redshift, $10''$ corresponds to 70.2 kpc. The quasar PSF has not been subtracted in this image.

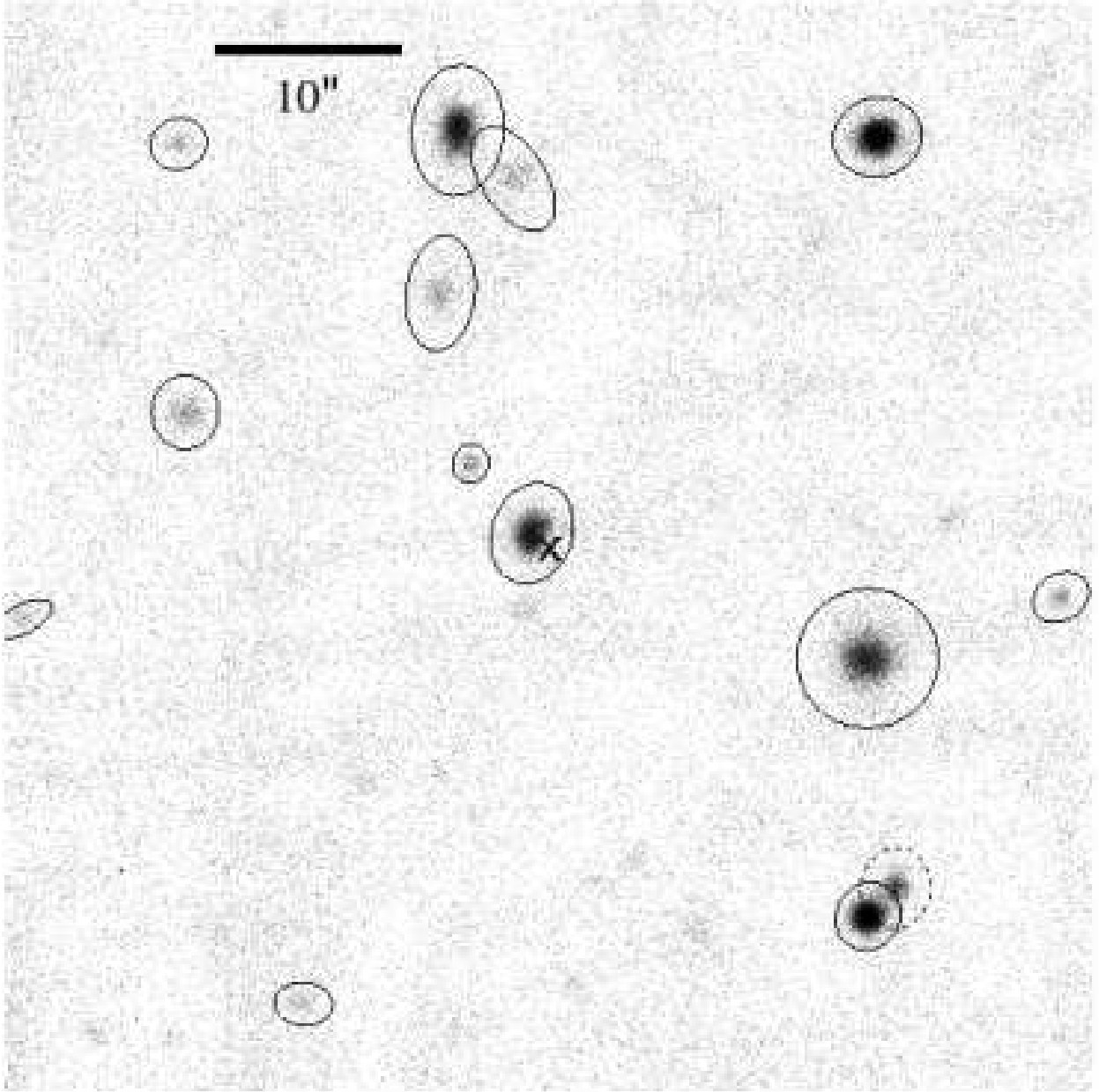


Fig. 10.— WIYN i' image of the Q1000+4438 field. The absorption has $z_{abs} = 0.7192$ and $W_0^{\lambda 2796} = 5.33 \text{ \AA}$. At the absorption redshift, $10''$ corresponds to 72.3 kpc.

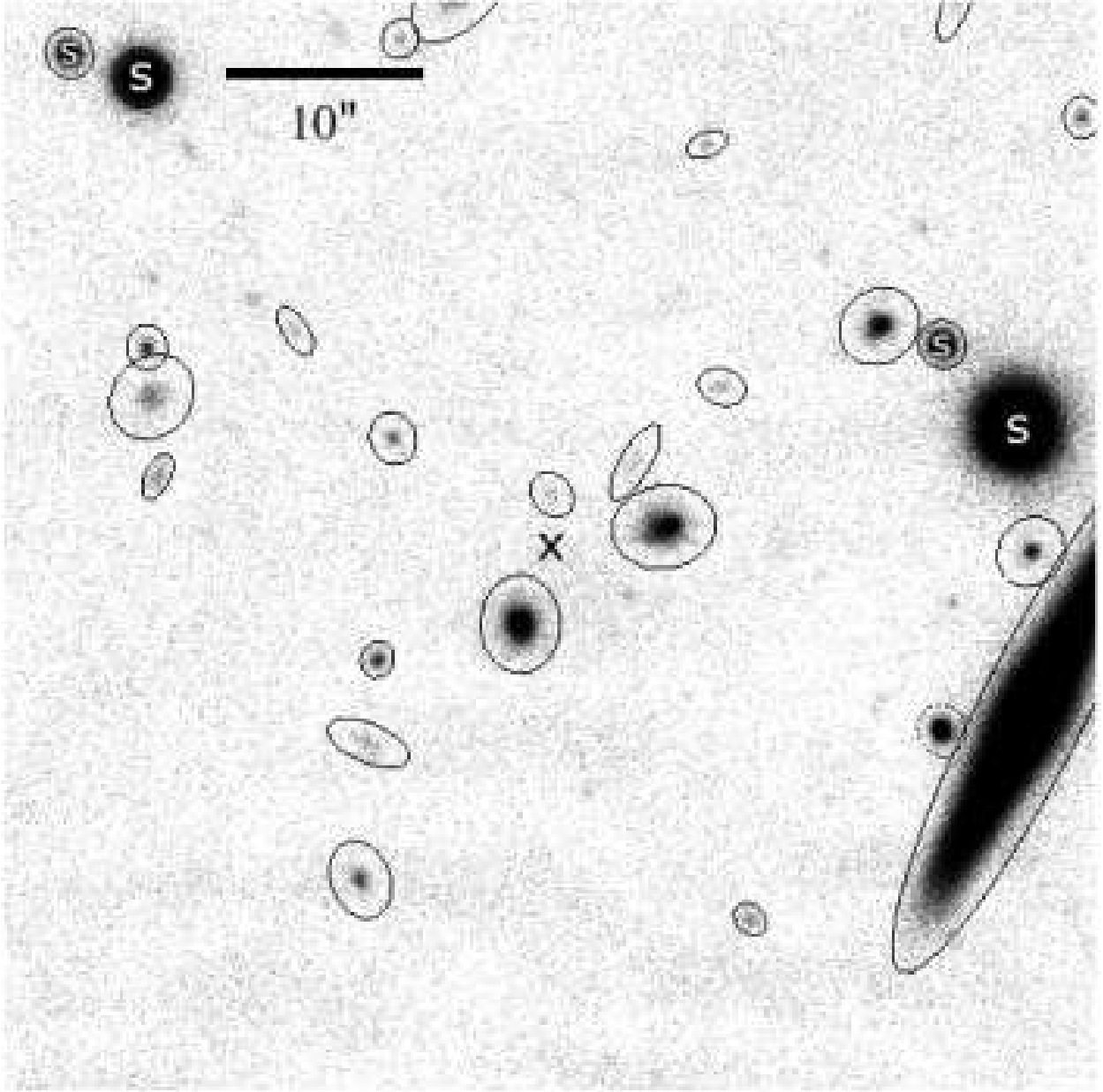


Fig. 11.— WIYN i' image of the Q1011+4451 field. The absorption has $z_{abs} = 0.8360$ and $W_0^{\lambda 2796} = 4.94 \text{ \AA}$. At the absorption redshift, $10''$ corresponds to 76.2 kpc.

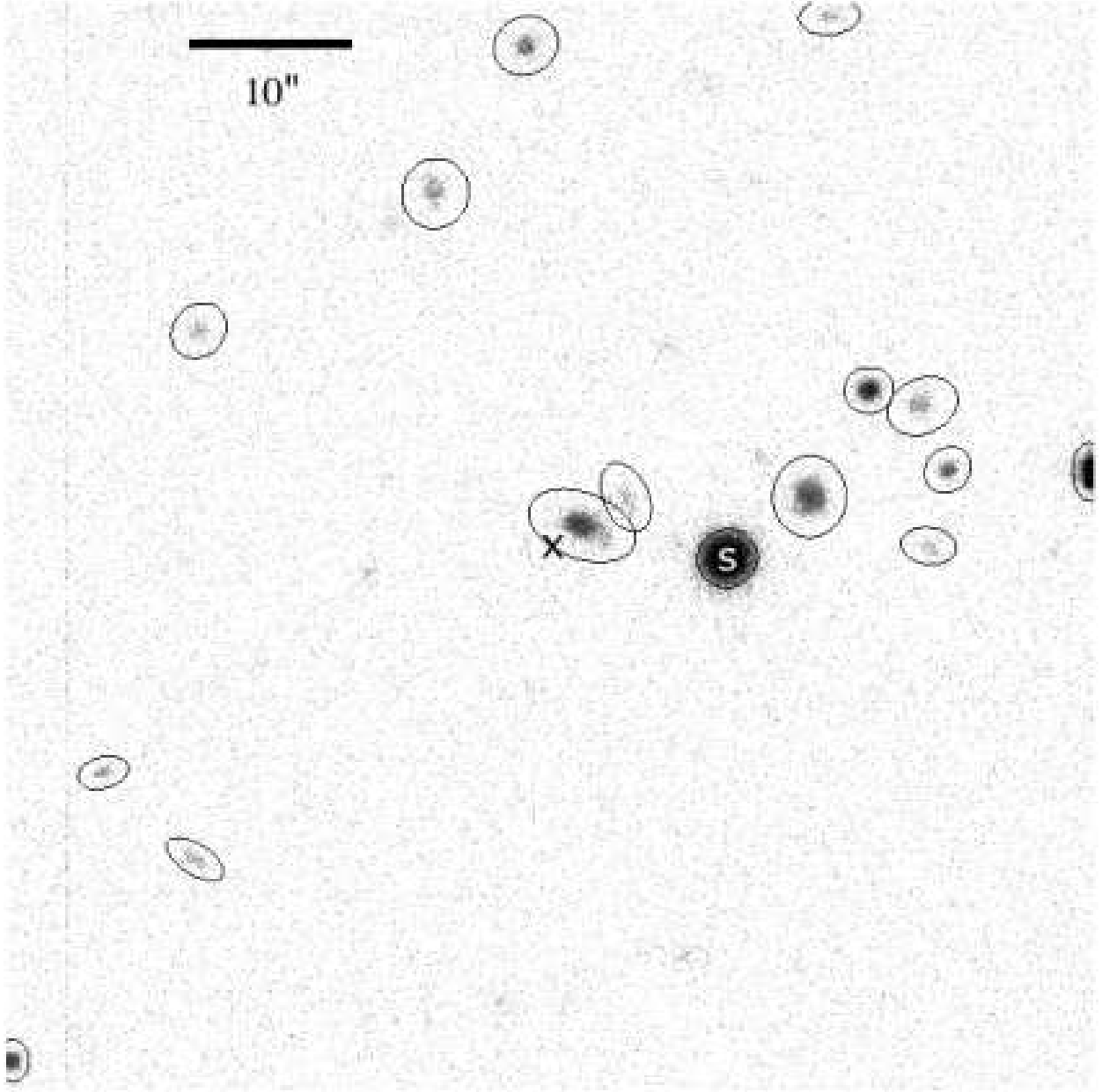


Fig. 12.— WIYN r' image of the Q1038+4727 field. The absorption has $z_{abs} = 0.5292$ and $W_0^{\lambda 2796} = 3.14 \text{ \AA}$. At the absorption redshift, $10''$ corresponds to 62.9 kpc.

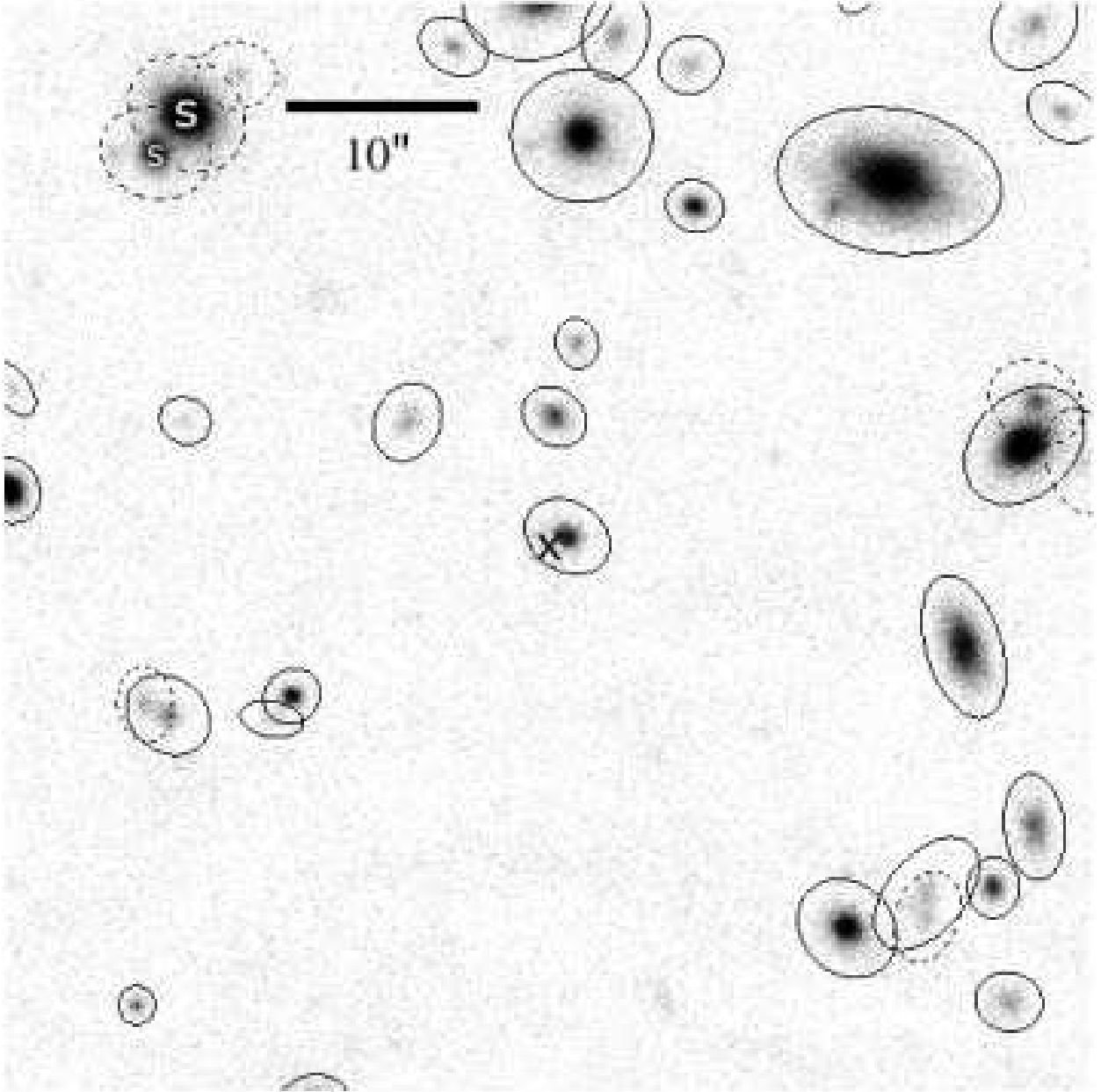


Fig. 13.— WIYN i' image of the Q1356+6119 field. The absorption has $z_{abs} = 0.7850$ and $W_0^{\lambda 2796} = 5.97 \text{ \AA}$. At the absorption redshift, $10''$ corresponds to 74.6 kpc.

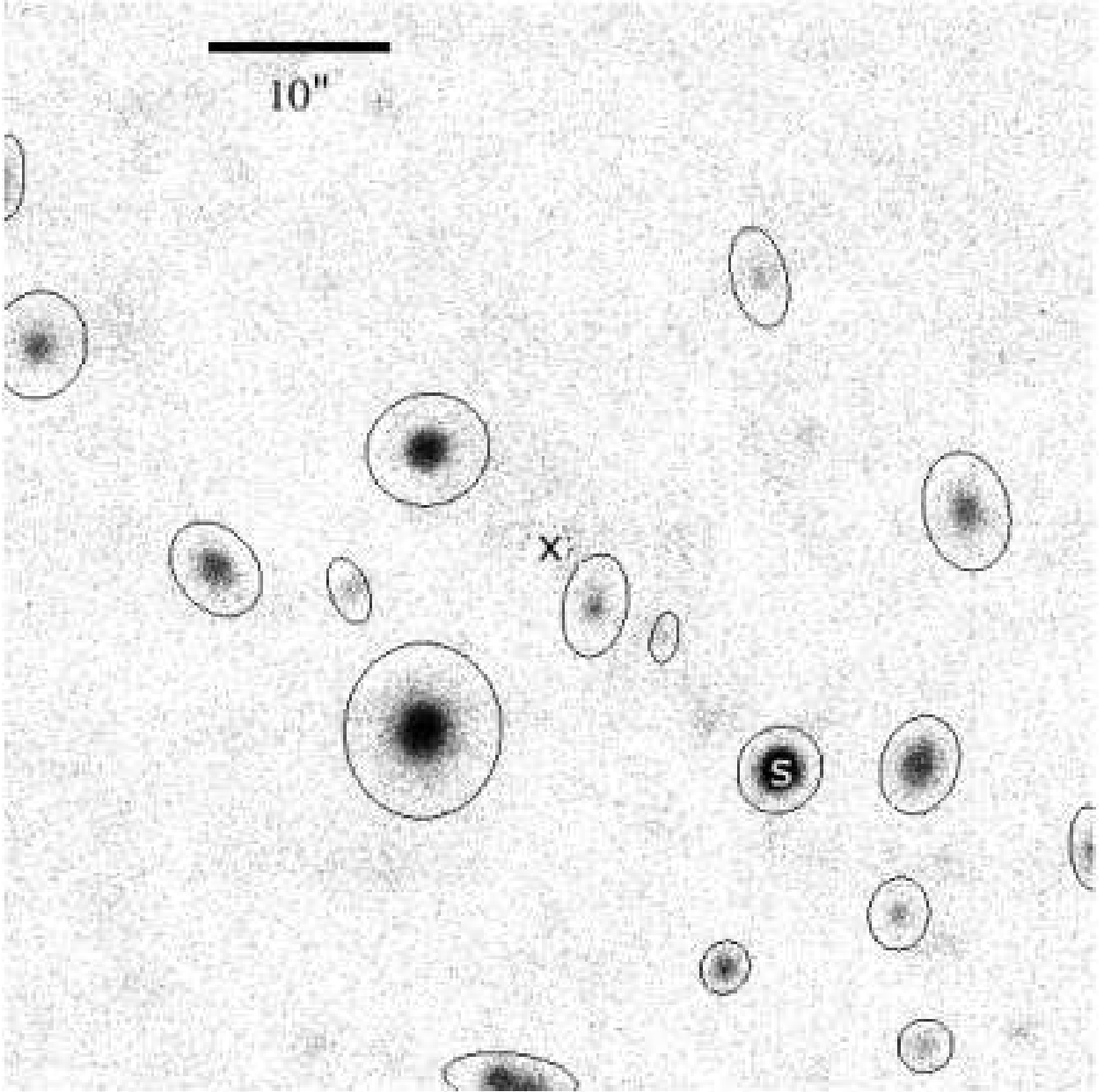


Fig. 14.— WIYN i' image of the Q1417+0115 field. The absorption has $z_{abs} = 0.6687$ and $W_0^{\lambda 2796} = 5.6 \text{ \AA}$. At the absorption redshift, $10''$ corresponds to 70.1 kpc.

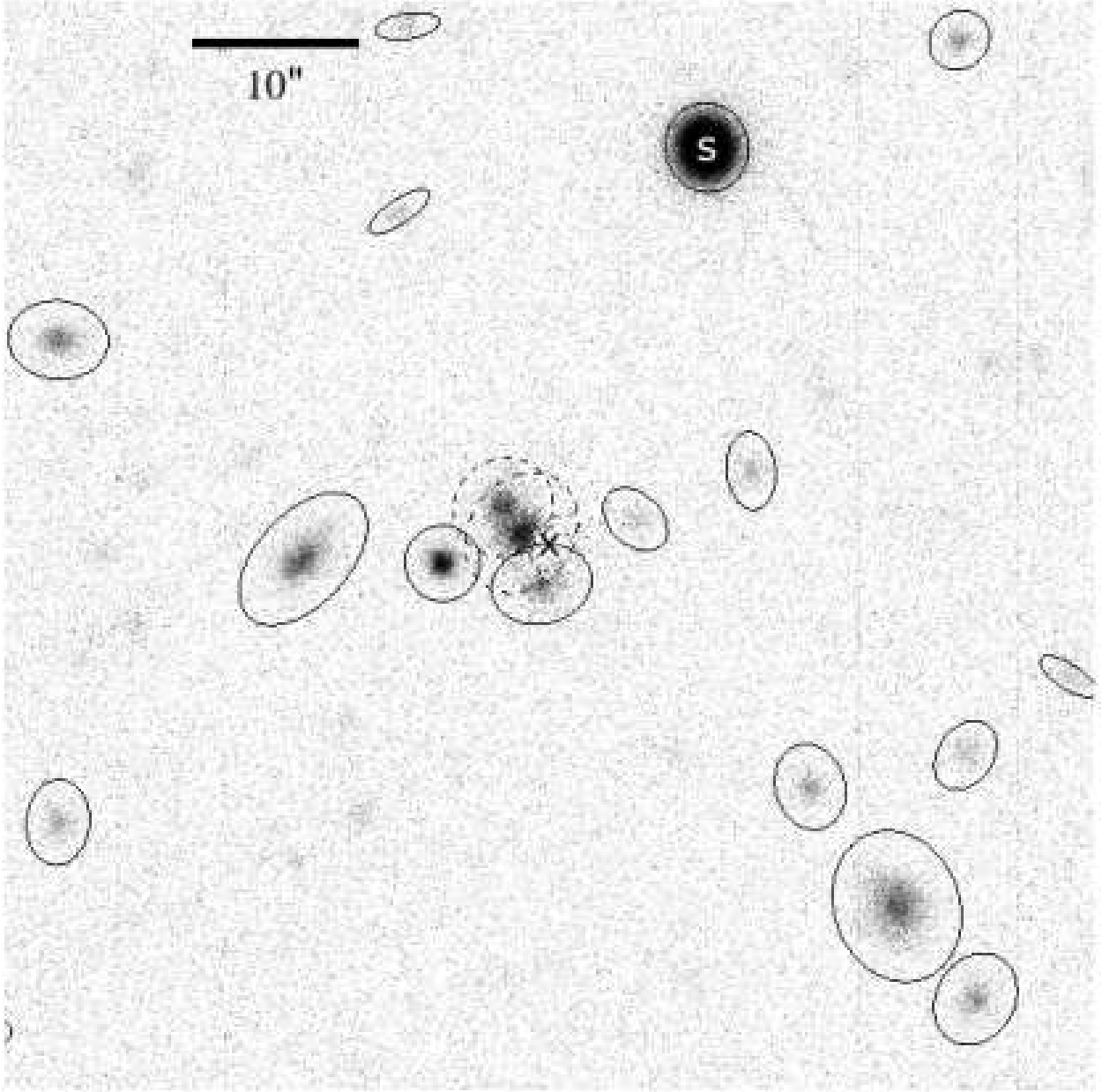


Fig. 15.— WIYN r' image of the Q1427+5325 field. The absorption has $z_{abs} = 0.5537$ and $W_0^{\lambda 2796} = 4.35 \text{ \AA}$. At the absorption redshift, $10''$ corresponds to 64.3 kpc.

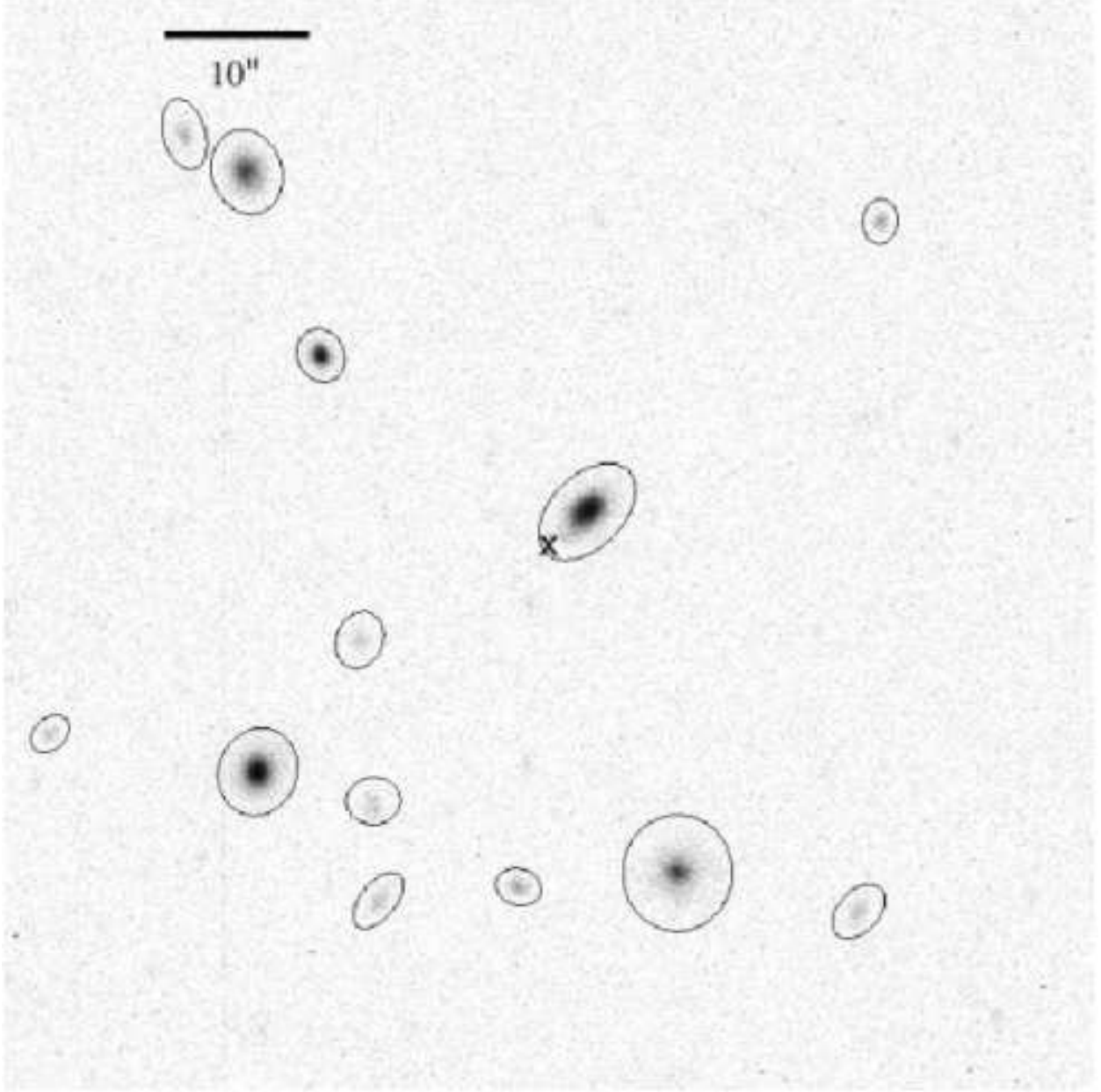


Fig. 16.— WIYN r' image of the Q1520+6105 field. The absorption has $z_{abs} = 0.4235$ and $W_0^{\lambda 2796} = 4.24 \text{ \AA}$. At the absorption redshift, $10''$ corresponds to 55.6 kpc.

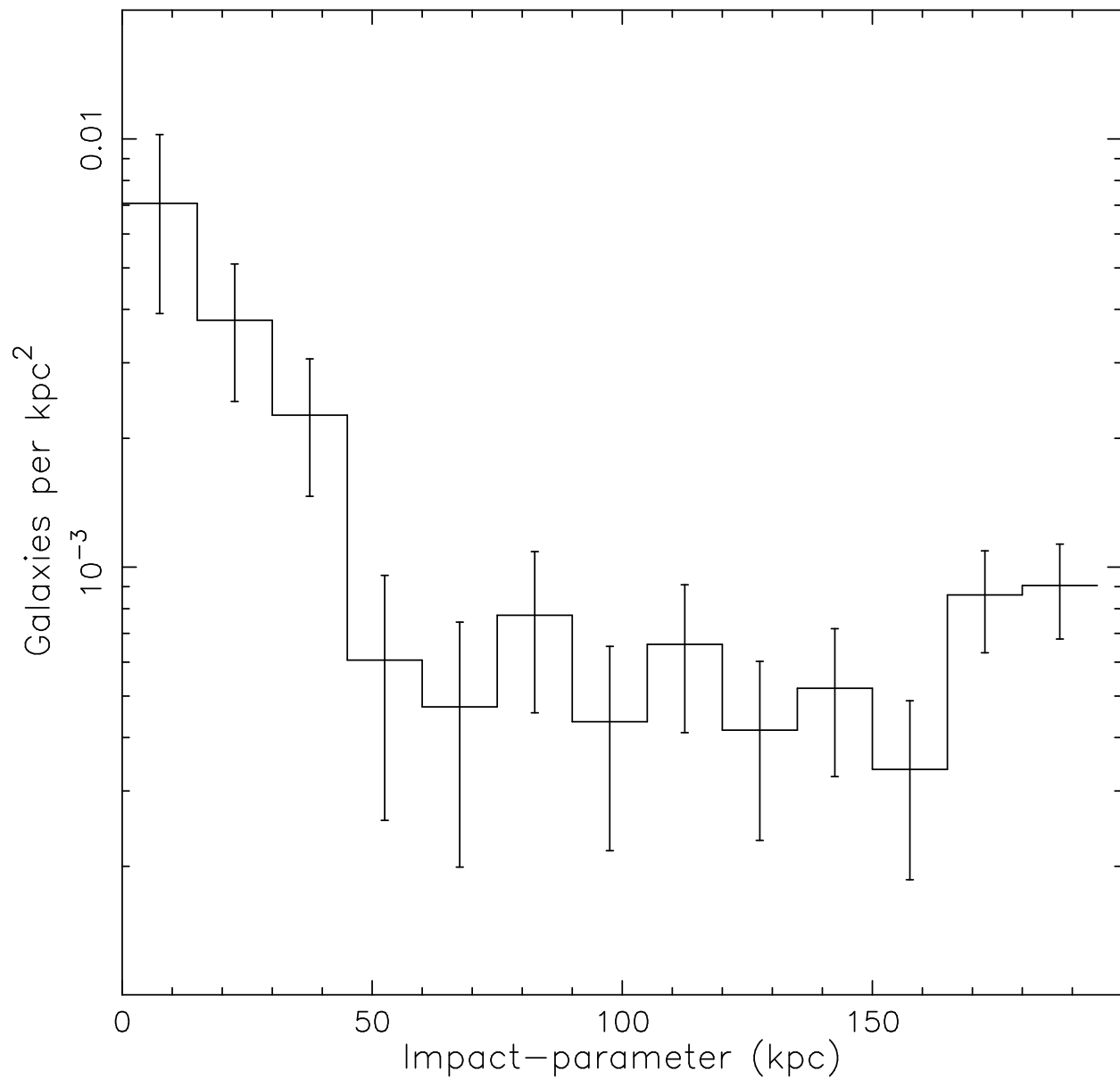


Fig. 17.— The surface-density of galaxies with $L(z = z_{abs}) \geq 0.5L^*$ in our fields as a function of impact parameter. There is a clear overdensity of galaxies with $b \lesssim 45$ kpc.

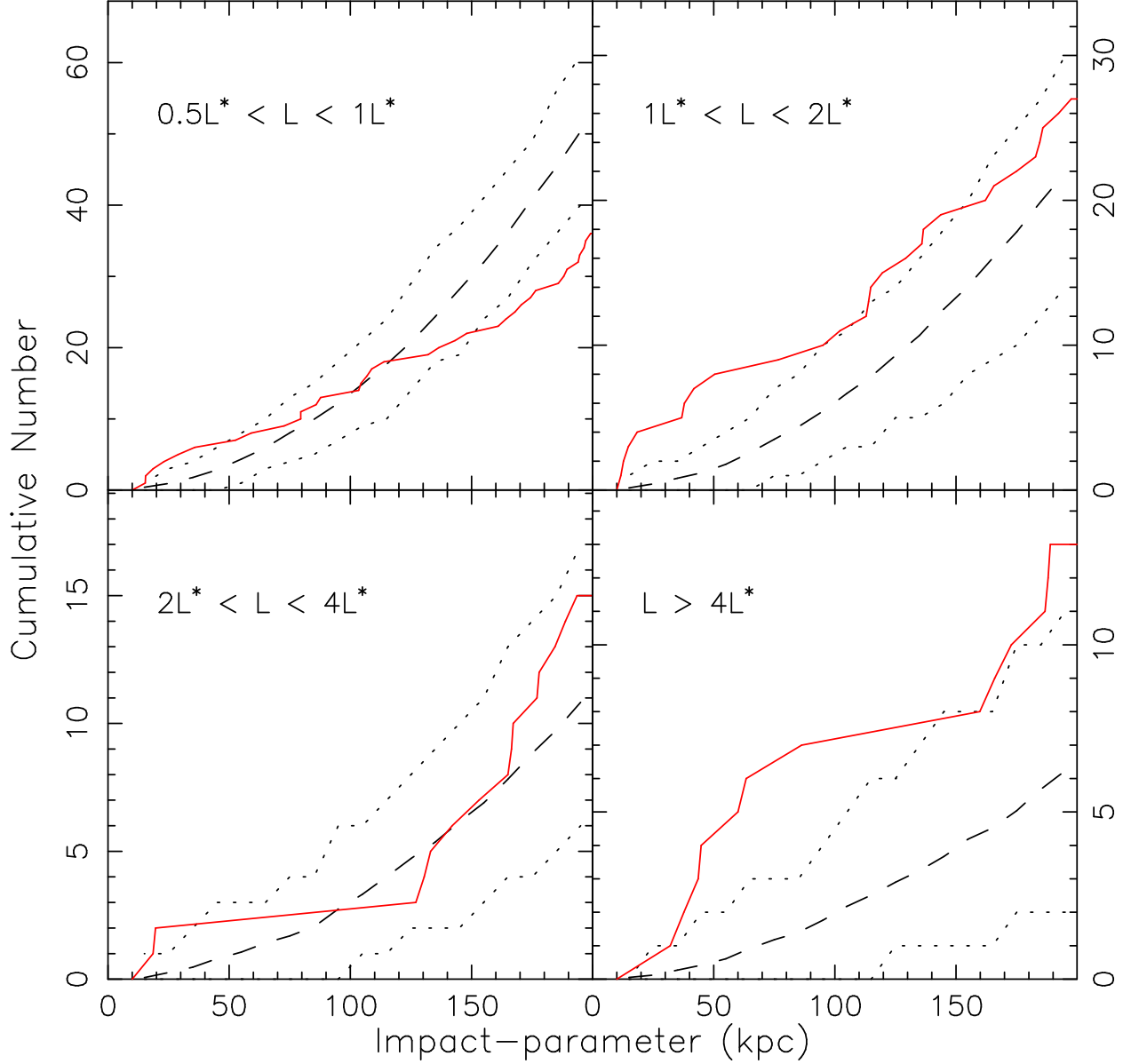


Fig. 18.— Cumulative distribution of galaxies as a function of impact parameter. The solid lines indicate the data. The dashed lines are the averages of 100 Monte Carlo simulations, and the dotted lines indicates the ranges containing 95% of the simulations. The excess/dearth of galaxies at any impact-parameter relative to the simulation can be seen by comparing the slopes of the curves. There is an excess of galaxies at low impact parameter for sources with $L(z = z_{abs}) \geq 0.5L^*$. The excess is particularly significant for $L(z = z_{abs}) \geq 4L^*$.

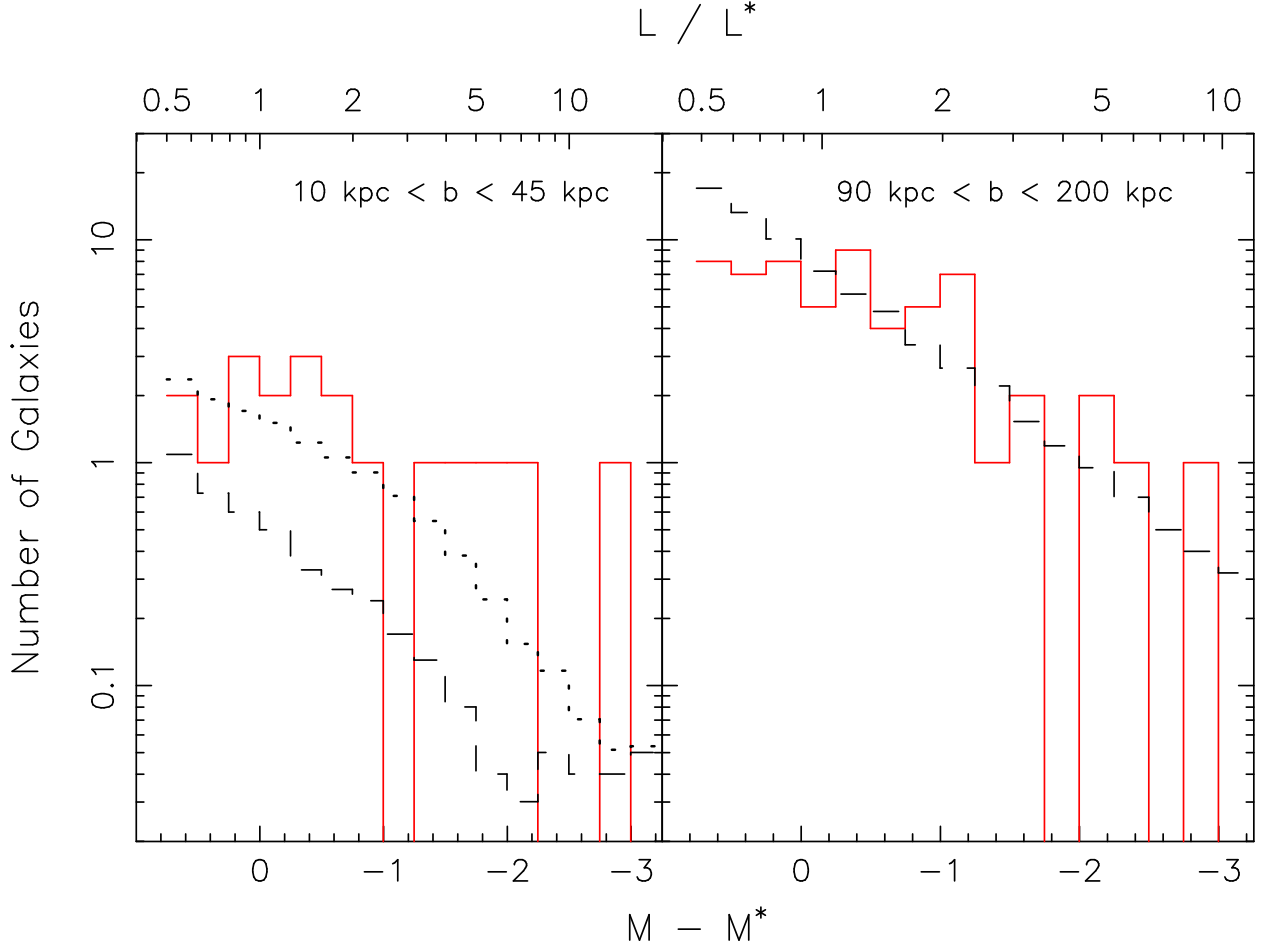


Fig. 19.— Distribution of galaxies having $L(z = z_{abs}) \geq 0.5L^*$ as a function of magnitude. The solid lines indicate the data. The dashed lines are the averages of 100 Monte Carlo simulations. Left: galaxies with impact parameters $10 \text{ kpc} < b < 45 \text{ kpc}$. There is a clear excess of galaxies compared to the simulations. The dotted line is the sum of the simulation result and the renormalized r' -band LF at $0.45 < z \leq 0.85$ from Gabasch et al. (2006). Right: galaxies with impact parameters $90 \text{ kpc} < b < 200 \text{ kpc}$. There is good agreement between the observed galaxy number-magnitude relation and the simulations, indicating that any correlation between absorbers and galaxies with $b > 90 \text{ kpc}$ is weaker than we can detect with our current sample.